J. Fluid Mech. (1990), *vol.* 217, *pp.* 391–420
Printed in Great Britain

Inviscid spatial stability of a compressible mixing layer. Part 2. The flame sheet model

By T. L. JACKSON[1] AND C. E. GROSCH[2]

[1] Department of Mathematics and Statistics, Old Dominion University, Norfolk, VA 23529, USA

[2] Department of Oceanography and Department of Computer Science, Old Dominion University, Norfolk, VA 23529, USA

(Received 16 May 1989 and in revised form 16 November 1989)

We report the results of an inviscid spatial stability calculation for a compressible reacting mixing layer. The limit of infinite Damkohler number is taken and the diffusion flame is approximated by a flame sheet. Results are reported for the phase speeds of the neutral waves and maximum growth rates of the unstable waves as a function of the parameters of the problem: the ratio of the temperature of the stationary stream to that of the fast stream, the Mach number of the fast stream, the heat release per unit mass fraction of the reactant, the equivalence ratio of the reaction, and the frequency of the disturbance. These results are compared to the phase speeds and growth rates of the corresponding non-reacting mixing layer. We show that the addition of combustion has important, and complex, effects on the flow stability. In particular, we show that the flow can become absolutely unstable with a sufficient amount of heat release.

1. Introduction

Quite recently it has been realized that an understanding of the stability characteristics of compressible mixing layers is extremely important in view of the projected use of the scramjet engine for the propulsion of hypersonic aircraft. For example, Drummond & Mukunda (1988) state: 'Even though the combustor flow field is quite complex, it can be realistically viewed as a collection of spatially developing and reacting supersonic mixing layers that are initially discrete, but that ultimately merge into larger more complex zones. These mixing layers begin downstream of a set of fuel injectors that introduce gaseous hydrogen in both a parallel and transverse direction into a supersonic airstream entering from the engine inlet. The behaviour of the initial portion of the combustor flow, in the mixing layers near the fuel injectors, appears to be most critical, since this is where the mechanism for efficient high speed mixing must be established to achieve the required degree of combustion downstream. Because of the structure of the flow field in this initial portion of the combustor, a single supersonic, spatially developing and reacting mixing layer serves as an excellent physical model for the overall flow field.' Thus, knowledge of the stability characteristics may allow one, in principle, to control the downstream evolution of such flows in the combustor. This is particularly important because of the observed increase in the flow stability at high Mach numbers (Brown & Roshko 1974; Chinzei *et al.* 1986; Papamoschou & Roshko 1986, 1988). Because of

the increase in stability, natural transition may occur at downstream distances which are larger than practical combustor lengths. A number of techniques which may enhance mixing are discussed by Kumar, Bushnell & Hussaini (1987). A detailed understanding of the linear stability characteristics of compressible reacting mixing layers will be of aid in mixing enhancement.

Despite the fact that understanding of the flow field in a reacting compressible mixing layer in a scramjet engine is extremely important, there appear to be very few studies of the stability of such flows. Menon, Anderson & Pai (1984) studied the inviscid spatial stability of a compressible wake in which there was a H_2–O_2 reaction. These calculations were carried out with a free-stream Mach number of 2 and temperature of 1500 K. When the reaction was turned on, the flow became completely unstable. The phase speed was found to be a monotonically increasing function of frequency. It seems that their results show a complete absence of neutral or stable disturbances.

The above result appears to be in conflict with that of Drummond & Mukunda (1988). They carried out a numerical simulation using the two-dimensional, compressible, time dependent Navier–Stokes equations with combustion in a mixing layer. The reaction was the burning of a 10% H_2, 90% N_2 fuel in air. The free-stream Mach number was taken to be 2, the temperature above and below the plate was 2000 K, and the velocities were 2672 m/s and 1729 m/s above and below the plate, respectively. Because of the expense and difficulty of carrying out these simulations only a few have been done. Drummond & Mukunda found that the non-reacting flow was very stable and that turning on the combustion had little effect. But it should be noted that the authors were not carrying out a stability calculation, *per se*, and did not excite the flow with disturbances with a fixed frequency. They relied on 'natural' disturbances to perturb the flow.

Recently, Hermanson & Dimotakis (1989) carried out an experimental study of the effect of heat release in a turbulent shear layer at low subsonic speeds. Among their findings were that the growth rate of the layer decreases slightly with increasing heat release. McMurtry, Riley & Metcalfe (1989) carried out three-dimensional, time dependent simulations of a reacting mixing layer in the zero-Mach-number limit. Similarly, they found that increasing the heat release led to a decrease in the growth rate of the mixing layer.

We have begun a systematic study of the stability of compressible mixing layers in which a diffusion flame is embedded. The basic steady flow with which we began is that calculated by Jackson & Hussaini (1988). In their study the limit of infinite activation energy was used and the diffusion flame reduced to a flame sheet. The flame sheet model is a standard approximation and has been used in the study of the burning of a fuel particle in an oxidizing atmosphere and of the flame at the mouth of a tube, for example (Buckmaster & Ludford 1982; Williams 1985). In order to understand the effect of the chemical heat release on the stability of this flow, one must first understand the stability characteristics of the non-reacting flow.

In the first part of our study (Jackson & Grosch 1989, hereinafter referred to as Part 1), we considered the inviscid spatial stability problem for the compressible mixing layer with the mean velocity profile approximated by the hyperbolic tangent. We found that there is only a single subsonic neutral mode for two-dimensional waves, but that there can be three for three-dimensional waves. Beyond a critical Mach number M_s, the Mach number at which the phase speed equals that of a sonic wave, the subsonic neutral modes are transformed into supersonic neutral modes which are subsonic at one boundary and supersonic at the other (we have not found

any neutral or unstable modes which are supersonic at both boundaries). In addition, another supersonic neutral mode appears at $M_* \geqslant M_s$, the Mach number at which the sonic speeds of the stationary and moving streams are equal. This supersonic neutral mode has the opposite behaviour to the previous one at the boundaries. That is, if the continuation of the subsonic neutral mode is supersonic in the moving stream and subsonic in the stationary stream, this new mode is subsonic in the moving stream and supersonic in the stationary stream. Thus, there are always at least two bands of unstable frequencies for Mach numbers greater than M_*. One of these bands is a group of fast and the other a group of slow unstable supersonic modes. The fast modes are supersonic with respect to the stationary stream and the slow modes are supersonic with respect to the moving stream. It is important to note that both the fast and slow supersonic modes are vorticity modes and neither of them is an acoustic mode (Mack 1989). These groups of unstable modes lie in the frequency bands between zero, corresponding to the sonic mode, and the frequency of the supersonic neutral mode. Because these frequency bands always overlap for some range of frequencies, there exist two unstable modes at a fixed Mach number and β_T (the ratio of the temperature in the stationary stream to that of the moving stream) for every frequency in this range. The phase speeds of both the fast and slow supersonic modes have a small range about the average, so that little dispersion of wave packets is expected, with a reduction in the dispersion as the Mach number is increased. Three-dimensional disturbances show the same general characteristics as two-dimensional disturbances. There is always a range of propagation angles for which both the fast and slow unstable modes exist. We also find, in agreement with previous studies, that the maximum growth rate for any β_T and M occurs for three-dimensional waves. A decrease in β_T results in an increase in the growth rate of the unstable waves at any Mach number. An increase in the Mach number at a fixed β_T results in a decrease of the growth rates by a factor of five to ten, until the Mach number equals M_*. For Mach numbers greater than M_*, the growth rates of all modes level off and then, with increasing Mach number, those of the slow modes begin to increase while those of the fast modes approach a limiting value. However, even at Mach 10, the growth rates of the slow modes are still small compared to those at low subsonic speeds. This, combined with the fact that the unstable waves have little dispersion, is a possible mechanism responsible for the observed increase in the flow stability.

In this paper we report results of a study of the stability of a reacting compressible mixing layer. In §2 we give the basic equations governing the mean flow and the small amplitude disturbance equations. The boundary conditions and the numerical method are also discussed in this section. Section 3 contains a presentation of our results and conclusions are given in §4.

2. The mean flow

The non-dimensional equations governing the steady two-dimensional flow of a compressible, reacting mixing layer which lies between streams of reactants with different speeds and temperatures are given by (Jackson & Hussaini 1988)

$$(\rho U)_x + (\rho V)_y = 0, \quad 1 = \rho T, \tag{2.1a, b}$$

$$\rho(UU_x + VU_y) = (\mu U_y)_y, \tag{2.1c}$$

$$\rho(UT_x + VT_y) = (\mu T_y)_y + (\gamma - 1)M^2 \mu U_y^2 + \beta\Omega, \tag{2.1d}$$

$$\rho(UF_{j_x} + VF_{j_y}) = (\mu F_{j_y})_y - \beta_j \Omega \quad (j = 1, 2). \tag{2.1e}$$

In these equations the x-axis is along the direction of flow, the y-axis is normal to the flow, U and V are the velocity components in the x- and y-directions, respectively, ρ is the density, T the temperature, F_1 and F_2 the mass fractions, and Ω is the reaction rate. The viscosity μ is given by Chapman's linear viscosity law. The other non-dimensional parameters appearing above are:

$$\beta = QF_{1,\infty}\hat{\nu}W/C_p T_\infty(\hat{\nu}_1-\hat{\mu}_1)W_1 \quad \text{Heat release per unit mass fraction of reactant,}$$

$$\beta_j = (\hat{\nu}_j-\hat{\mu}_j)W_j/(\hat{\nu}_1-\hat{\mu}_1)W_1 \quad \text{Parameter involving stoichiometry,}$$

$$M = U_\infty/a_\infty \quad \text{Mach number,}$$

where $\hat{\nu}_j$ is the stoichiometric coefficient for species j appearing as a reactant, $\hat{\mu}_j$ the stoichiometric coefficient for species j appearing as a product, $\hat{\nu}$ the sum of the stoichiometric coefficients of the reactants, W_j the molecular weight of species j, W the average molecular weight, a_∞ the speed of sound referred to T_∞, Q the chemical heat release per unit mass, γ the specific-heat ratio, and finally C_p the specific heat at constant pressure. The equations were non-dimensionalized by the free-stream values $T_\infty, \rho_\infty, U_\infty, F_{1,\infty}$ for the temperature, density, velocities and mass fractions, respectively. Lengths are referred to some characteristic lengthscale of the flow. We have assumed unit Prandtl and Lewis numbers in writing down these equations. The assumption of unit Lewis number allows us to consider linear combinations of (2.1d) and (2.1e) to eliminate the source term, which then admits similarity-type solutions. For a simplified hydrogen–oxygen reaction, typical values of the heat release parameter β as a function of the temperature of the fast stream are given in table 1. Note that as the temperature of the fast stream is increased, β is decreased.

The boundary conditions consistent with (2.1) are

$$T = U = F_1 = 1, \quad F_2 = 0 \quad \text{as } y \to \infty, \tag{2.2a}$$

$$T = \beta_T, U = \beta_U < 1, \quad F_1 = 0, \quad F_2 = \frac{F_{2,-\infty}}{F_{1,\infty}} \quad \text{as } y \to -\infty. \tag{2.2b}$$

If β_T is less than one, the slow gas is relatively cold compared to the fast stream, and if β_T is greater than one it is relatively hot.

The linear combinations

$$T+\beta F_1, \quad T+\frac{\beta}{\beta_2}F_2, \tag{2.3}$$

satisfy pure heat equations everywhere, which admit similarity type solutions. Combining (2.1d) and (2.1e), and using the boundary conditions (2.2), one finds

$$T+\beta F_1 = \beta_T + (1-\beta_T+\beta)\left(\frac{U-\beta_U}{1-\beta_U}\right) + \tfrac{1}{2}(\gamma-1)M^2(U-\beta_U)(1-U), \tag{2.4a}$$

$$T+\frac{\beta}{\beta_2}F_2 = \beta_T + \beta\phi^{-1} + (1-\beta_T-\beta\phi^{-1})\left(\frac{U-\beta_U}{1-\beta_U}\right) + \tfrac{1}{2}(\gamma-1)M^2(U-\beta_U)(1-U), \tag{2.4b}$$

where ϕ is the equivalence ratio, defined by

$$\phi = \frac{F_{1,\infty}/F_{2,-\infty}}{\beta_1/\beta_2}, \tag{2.5}$$

which is the ratio of the mass fraction F_1 in the fast stream to the mass fraction F_2 in the slow stream divided by the ratio of their molecular weights times their

T_∞ (°K)	C_p (cal/mole °K)	$Q\hat{\nu}W/\hat{\nu}_1 W_1$ (kcal/mole)	β
1000	9.03	516.5	3.2
1500	9.94	516.5	1.9
2000	10.60	516.5	1.4

TABLE 1. Typical values of the heat release parameter β as a function of temperature

stoichiometric coefficients. Note that if $\phi = 1$, then the mixture is said to be stoichiometric, and if $\phi > 1$ it is F_1 rich, while if $\phi < 1$ it is F_1 lean.

A thin diffusion flame exists within the mixing layer and is characterized by near-equilibrium conditions; $F_1 = 0$ on one side of the flame and $F_2 = 0$ on the other. In the limit of infinite Damkohler number this thin diffusion flame reduces to a flame sheet and from the relations (2.4), we see that the flow can be described by

$$F_1 = 1-(1+\phi^{-1})\left(\frac{1-U}{1-\beta_U}\right), \quad F_2 = 0, \tag{2.6a}$$

$$T = \beta_T+\beta\phi^{-1}+(1-\beta_T-\beta\phi^{-1})\left(\frac{U-\beta_U}{1-\beta_U}\right)+\tfrac{1}{2}(\gamma-1)M^2(U-\beta_U)(1-U), \tag{2.6b}$$

for $y > y_f$, and

$$F_1 = 0, \quad F_2 = \frac{\beta_2}{\beta_1}\left[\phi^{-1}-(1+\phi^{-1})\left(\frac{U-\beta_U}{1-\beta_U}\right)\right], \tag{2.7a}$$

$$T = \beta_T+(1-\beta_T+\beta)\left(\frac{U-\beta_U}{1-\beta_U}\right)+\tfrac{1}{2}(\gamma-1)M^2(U-\beta_U)(1-U), \tag{2.7b}$$

for $y < y_f$. Here, y_f gives the location of the flame sheet where both reactants vanish, and T takes the adiabatic flame value T_f, given by

$$T_f = \beta_T+(1-\beta_T+\beta)\left(\frac{U_f-\beta_U}{1-\beta_U}\right)+\tfrac{1}{2}(\gamma-1)M^2(U_f-\beta_U)(1-U_f), \tag{2.8}$$

and

$$U_f \equiv U(y_f) = \frac{1+\beta_U\phi}{1+\phi} \tag{2.9}$$

defines the flame location. Note that the flame location is independent of β_T and Mach number.

The temperature and mass fraction profiles for the steady mean flow have been obtained in terms of the mean flow velocity distribution, $U(y)$. As discussed in Part 1, we assume here that

$$U = \tfrac{1}{2}[1+\beta_U+(1-\beta_U)\tanh(\eta)], \tag{2.10}$$

where η is the similarity variable and the Howarth–Dorodnitzyn transformation has been used. This profile satisfies the boundary conditions

$$U \to 1 \quad \text{as } \eta \to +\infty, \quad U \to \beta_U < 1 \quad \text{as } \eta \to -\infty. \tag{2.11}$$

The basic mean flow considered here is thus given by (2.6), (2.7), and (2.10).

In figure 1(*a*) we show plots of $T(\eta)$ for $\beta_T = 2$, $\beta_U = 0$, $M = 0$, $\phi = 1$ and for various values of the heat release parameter β. If β is different from zero, the temperature always has a discontinuity in its slope at the location of the flame sheet.

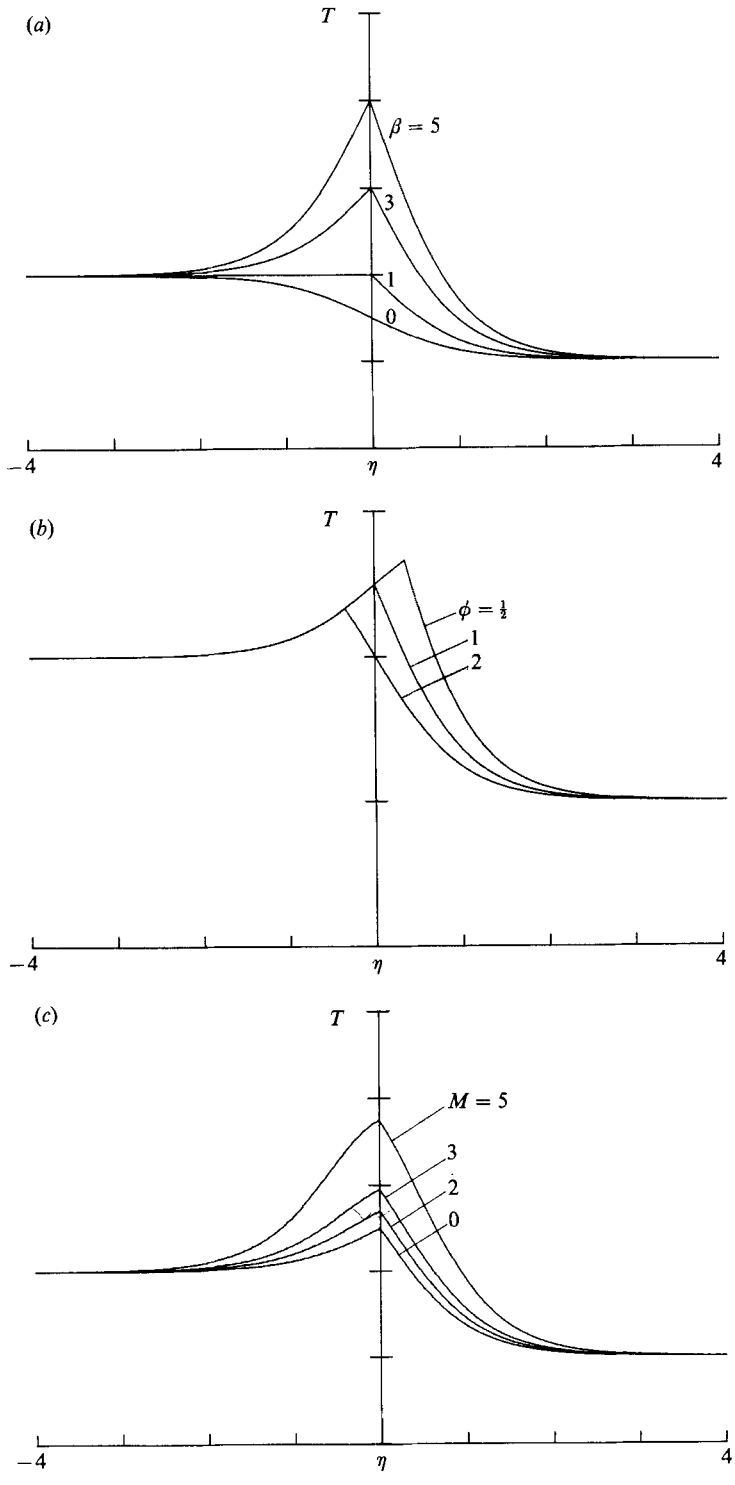

FIGURE 1. (a) Plot of temperature T versus η for $\beta_T = 2$, $\beta = 0, 1, 3, 5$, $\phi = 1$, and $M = 0$. (b) Plot of temperature T versus η for $\beta_T = 2$, $\beta = 2$, $\phi = 0.5, 1, 2$, and $M = 0$. (c) Plot of temperature T versus η for $\beta_T = 2$, $\beta = 2$, $\phi = 1$, and $M = 0, 2, 3, 5$.

Figure 1 (*b*) shows plots of T for $\beta_T = 2, \beta_U = 0, \beta = 2, M = 0$, and for various values of ϕ. When $\phi = 1$, the flame sheet is located at $\eta_f = 0$. For $\phi > 1$, the mixture is F_1 rich and the flame location shifts to $\eta_f < 0$. For $\phi < 1$, the converse is true. Finally, figure 1 (*c*) shows T for various values of the Mach number. As can be seen from (2.6)–(2.8), increasing M increases T. It should be noted that an increase in β at fixed M has a qualitatively similar effect on T as an increase in M at a fixed β.

The flow field is perturbed by introducing two-dimensional wave disturbances in the velocity, pressure, temperature, density and mass fractions on either side of the flame sheet with amplitudes which are functions of η. In addition, the flame sheet location must also be perturbed with a wave disturbance. For example, the pressure perturbation is

$$p = \Pi(\eta) \exp[\mathrm{i}(\alpha x - \omega t)], \tag{2.12}$$

with Π the amplitude. Here, for spatial stability α is complex. The real part of α is the wavenumber in the x-direction, while the imaginary part of α indicates whether the disturbance is amplified, neutral, or damped depending on whether α_{i} is negative, zero, or positive assuming positive group velocity. The frequency ω is taken to be real. Substituting the expression (2.12) for the pressure perturbation and similar expressions for the other flow quantities into the inviscid compressible equations yields the ordinary differential equations for the perturbation amplitudes. It is straightforward to derive a single equation governing Π, given by

$$\Pi'' - \frac{2U'}{U-c}\Pi' - \alpha^2 T[T - M^2(U-c)^2]\Pi = 0, \tag{2.13}$$

which is valid on either side of the flame sheet. Here, c is the complex wave velocity

$$c = \omega/\alpha, \tag{2.14}$$

and primes indicate differentiation with respect to the similarity variable η. The phase speed, c_{ph}, is given by $\omega/\alpha_{\mathrm{r}}$. For a neutral wave the phase speed will be denoted by c_{N}.

The boundary conditions for Π are obtained by considering the limiting form of (2.13) as $\eta \to \pm\infty$. The solutions to (2.13) are of the form

$$\Pi \to \exp(\pm \Omega_{\pm} \eta), \tag{2.15}$$

where

$$\Omega_+^2 = \alpha^2[1 - M^2(1-c)^2], \quad \Omega_-^2 = \alpha^2 \beta_T[\beta_T - M^2(\beta_U - c)^2]. \tag{2.16}$$

Let us define $c_{\pm}$ to be the values of the phase speed for which $\Omega_{\pm}^2$ vanishes. Thus,

$$c_+ = 1 - \frac{1}{M}, \quad c_- = \beta_U + \frac{(\beta_T)^{\frac{1}{2}}}{M}. \tag{2.17}$$

Note that c_+ is the phase speed of a sonic disturbance in the fast stream and c_- is the phase speed of a sonic disturbance in the slow stream. At

$$M = M_* \equiv \frac{1 + (\beta_T)^{\frac{1}{2}}}{1 - \beta_U}, \tag{2.18}$$

$c_{\pm}$ are equal. In addition to the boundary conditions at $\eta = \pm\infty$, we must impose the conditions that Π and Π' are continuous across the flame sheet.

The nature of the disturbances and the appropriate boundary conditions can now be illustrated by reference to figure 2, where we plot $c_{\pm}$ versus M for a typical value of β_T and β_U. In what follows we assume that $\alpha_{\mathrm{r}}^2 > \alpha_{\mathrm{i}}^2$. These curves divide the $c_{\mathrm{r}} - M$

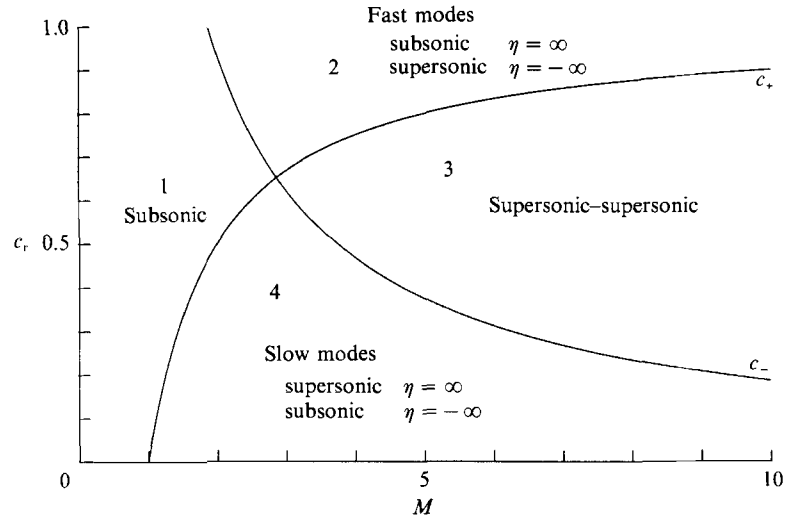

FIGURE 2. Plot of the sonic speeds $c_\pm$ versus Mach number for $\beta_T = 3.5$.

plane into four regions, where c_r is the real part of c. If a disturbance exists with a M and c_r in region 1, then Ω_+^2 and Ω_-^2 are both positive, and the disturbance is subsonic at both boundaries, and we classify it as a subsonic mode. In region 3, both Ω_+^2 and Ω_-^2 are negative and hence the disturbance is supersonic at both boundaries, and we classify it as supersonic–supersonic mode (or a doubly supersonic mode, the terminology of Macaraeg & Streett 1989). In region 2, Ω_+^2 is positive and Ω_-^2 is negative, and the disturbance is subsonic at $+\infty$ and supersonic at $-\infty$, and we classify it as a fast mode. Finally, in region 4, Ω_+^2 is negative and Ω_-^2 is positive so the disturbance is supersonic at $+\infty$ and subsonic at $-\infty$, and we classify it as a slow mode.

One can now see that the appropriate boundary condition for either damped or outgoing waves in the fast and slow streams are, respectively,

$$\Pi \to \exp(-\Omega_+ \eta) \quad \text{if } c_r > c_+, \quad \Pi \to \exp(-i\eta(-\Omega_+^2)^{\frac{1}{2}}) \quad \text{if } c_r < c_+, \tag{2.19a}$$

$$\Pi \to \exp(\Omega_- \eta) \quad \text{if } c_r < c_-, \quad \Pi \to \exp(-i\eta(-\Omega_-^2)^{\frac{1}{2}}) \quad \text{if } c_r > c_-. \tag{2.19b}$$

To solve the disturbance equation (2.13), we first transform it to a Riccati equation by setting

$$G = \frac{\Pi'}{\alpha T \Pi}. \tag{2.20}$$

Thus, (2.13) becomes

$$G' + \alpha T G^2 - \left(\frac{2U'}{U-c} - \frac{T'}{T}\right) G = \alpha[T - M^2(U-c)^2]. \tag{2.21}$$

The boundary conditions can be found from (2.19) and (2.20), with G continuous across the flame sheet.

The stability problem is thus to solve (2.21) for a given real frequency ω and Mach number M, with U and T defined by (2.10) and (2.6b), (2.7b). In addition to M, the important parameters of this problem are β_U, β_T, β, and ϕ. The eigenvalue is the wavenumber α. Because this equation has a singularity at $U = c_N$, we shall integrate it along the complex contour $(-6, -1)$ to $(\eta_f, 0)$ and $(6, -1)$ to $(\eta_f, 0)$, where η_f gives the flame sheet location defined by (2.9). Using a Runge–Kutta scheme with variable

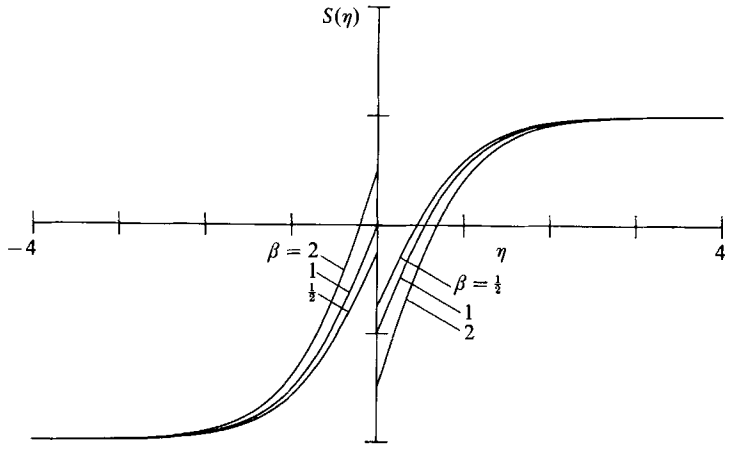

FIGURE 3. Plot of $S(\eta)$ for $\beta_T = 2$, $\beta = 0.5, 1, 2$, $\phi = 1$, and $M = 0$.

step size, we choose an initial α and compute the boundary conditions from (2.19). We then iterate on α, using Muller's method, until the boundary conditions are satisfied and the jump in G at $(\eta_f, 0)$ is less than 10^{-6}. All calculations were done in 64-bit precision.

3. Results

In all of our calculations we have taken $\gamma = 1.4$; $\beta_T = 0.5, 1, 2$; $0 \leqslant \beta \leqslant 5$; $\phi = 0.5, 1, 2$; and $0 \leqslant M \leqslant 10$. In addition, we have taken $\beta_U = 0$ unless otherwise stated.

The Lees & Lin (1946) regularity condition is given by

$$S(\eta) \equiv \frac{\mathrm{d}}{\mathrm{d}\eta}\left(T^{-2}\frac{\mathrm{d}U}{\mathrm{d}\eta}\right) = 0. \tag{3.1}$$

Let η_c be a root of $S(\eta)$, and define $\tilde{c} = U(\eta_c)$. If $\tilde{c}$ lies in region 1 of the $c_r - M$ diagram (figure 2), then Lees & Lin have shown that, provided $\alpha \neq 0$, $\tilde{c} = c_N$ is the phase speed of a true neutral mode. The corresponding neutral wavenumber, α_N, must be determined numerically. The eigenfunction is called a subsonic neutral mode. If $\tilde{c}$ lies in regions 2, 3, or 4 of the $c_r - M$ diagram, then $\tilde{c}$ does not correspond to the phase speed of a true neutral mode. The phase speeds in these regions must be found numerically. In addition to the neutral modes with $\alpha \neq 0$ there may exist neutral modes having zero wavenumber. These may exist in any of the four regions of figure 2. The phase speeds of such modes do not satisfy (3.1) and must be found numerically. In this zero wavenumber case, the amplitude of the V perturbation eigenfunction is $U - c$, or in terms of the pressure perturbation, $\Pi =$ constant. The correct value of c is not arbitrary but is found numerically in the limit $\alpha \to 0, \omega \to 0$. These modes do not exist in the non-reactive case, but do exist when the flame sheet is present.

Because T' is discontinuous at η_f for non-zero β, $S(\eta)$ will also be discontinuous at this point. Figure 3 is a plot of S versus η for various values of β. As one can see from examination of this figure, S can have a single root, two roots one of which corresponds to η positive and the other negative, or two roots one of which is a one-sided zero. The roots of S, which corresponds to phase speeds that are subsonic at

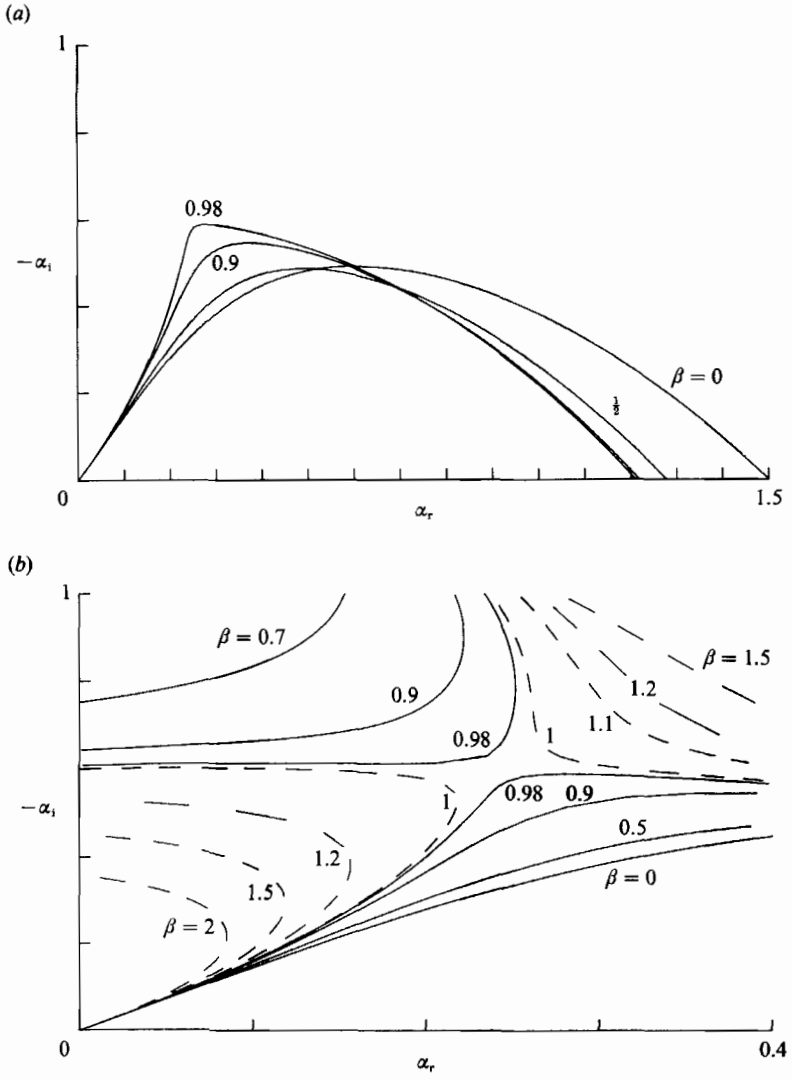

FIGURE 4(*a*,*b*). For caption see facing page.

both boundaries, are the phase speeds of subsonic neutral modes. The one-sided zero of S may or may not yield a phase speed of a neutral mode.

3.1. $M = 0$

The introduction of a chemical reaction, in the form of a flame sheet, has complex effects on the flow stability. In order to show these effects clearly, we first consider the case of zero Mach number and examine the variation of the eigenvalue, α, with the heat release parameter β and equivalence ratio ϕ. In figure 4(*a*) we show a plot of the growth rate ($-\alpha_i$) versus the real part of the wavenumber (α_r) for the case of $\beta_T = 0.5, \phi = 1$, and various values of β. Note that all of the curves pass through the origin, which corresponds to $\omega = 0$, and also cross the α_r axis, corresponding to $\omega > 0$. These give the two neutral modes. The phase speed corresponding to $\omega = 0$, $\alpha = 0$ does not correspond to a root of (3.1), while the phase speed corresponding to $\omega > 0$ is that of a subsonic neutral mode (whose phase speed is given by the Lees &

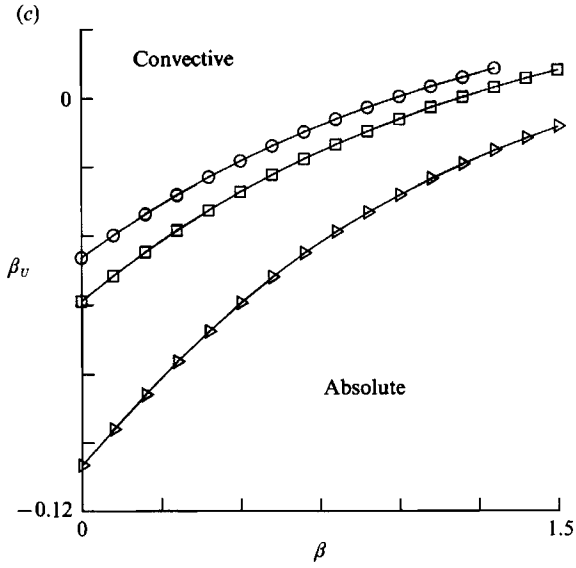

FIGURE 4. (*a*) Plot of the growth rate ($-\alpha_i$) versus the real part of the wavenumber (α_r) for $\beta_T = 0.5$, $\beta = 0, 0.5, 0.9, 0.98$, $\phi = 1$, and $M = 0$. (*b*) Plot of the growth rate ($-\alpha_i$) versus the real part of the wavenumber (α_r) for $\beta_T = 0.5$, $\phi = 1$, $M = 0$, and various values of β about the saddle-point location. (*c*) Plot of the curves separating regions of absolute and convective instability in the $\beta_U - \beta$ plane for Mach numbers of ○, 0; □, 0.5; △, 1.0 with $\phi = 1$.

Lin regularity condition (3.1)). Note that the stability curves of the unstable modes are found between two neutral modes.

The curves shown in figure 4(*a*) are for values of $\beta \leqslant 0.98$. For this particular set of parameter values we were not able to find solutions to the stability problem whose eigenvalues had the behaviour shown in this figure for any values of $\beta > 0.983$. In order to understand the reason for this we carried out an extensive search for eigenvalues in the α-plane while varying β. We discovered that the eigenvalue problem has a saddle point in the α-plane. Figure 4(*b*) shows the region about the saddle point, which occurs for β about 0.984 at $\alpha = 0.24$–0.60i. For $\beta < 0.984$ there are two sets of eigenvalue curves. The lower set yields the eigenvalue relation for the non-reacting mixing layer as β approaches zero. For $\beta > 0.984$ there are also two other sets of eigenvalue curves.

Huerre & Monkewitz (1985) have pointed out that an occurrence of a saddle point may be related to a transition from convective to absolute instability.† If such a transition occurs the spatial stability theory is no longer appropriate and temporal calculations are now required. In the non-reacting case, Huerre & Monkewitz (1985) have shown that the incompressible mixing layer is convectively unstable for β_U non-negative. This result was extended to the subsonic compressible case by Pavithran & Redekopp (1990) and Jackson & Grosch (1990) independently. We have extended this analysis to include the flame sheet model. Our results are shown in figure 4(*c*) wherein we plot the locus of the branch point position separating the regions of absolute and convective instability in the $\beta_U - \beta$ plane for various Mach numbers. In the region above each curve the flow is convectively unstable while in the region below the flow is absolutely unstable. One can see from this figure that the transition

† We wish to thank P. A. Monkewitz, who suggested that the branch point might be connected to a transition from convective to absolute instability.

	ϕ		
β_T	0.5	1.0	2.0
0.5	0.7	0.984	1.8
1.0	2.0	3.1	>5
2.0	>5	>5	>5

TABLE 2. Typical values of β_c at $M = 0$ and $\beta_U = 0$ as a function of β_T and ϕ

from convective to absolute instability, at $\beta_U = 0$, occurs at $\beta \approx 0.984$ at zero Mach number. This value of β corresponds to the saddle point value found in figure 4(*b*) mentioned above. Thus the lower set of branches corresponds to the instability wave downstream of a time harmonic concentrated source, while the other branches (those existing with $\beta > 0.984$) represent the upstream influence of the source. This is also present in the homogeneous mixing layer as shown by Huerre & Monkewitz (1985). Finally, as the Mach number increases the critical value of β increases at any β_U. Most importantly, however, we note that the flow can be made absolutely unstable without any reversed flow for sufficiently large heat release.

We have found similar behaviour in the eigenvalue spectrum for other values of the parameters, for example, at $\beta_U = 0$ there is a critical value of β (β_c) beyond which transition from convective to absolute instability occurs. This value of β_c depends on all of the other parameters of the problem, and the general trends are similar. Typical values of β_c are given in table 2 as a function of β_T and ϕ. As β_T is increased, β_c also increases for fixed ϕ. As ϕ is increased, β_c also increases for fixed β_T. Thus it is possible to induce absolute instability by either increasing the heat release parameter β, or by decreasing the equivalence ratio ϕ (i.e. lean mixtures), holding all other parameters fixed. In the remainder of this paper we only present results for modes which are convectively unstable.

3.1.1. *Neutral modes*

In figures 5, 6 and 7 we show the variation of the neutral phase speeds c_N with β for various values of β_T and ϕ. First, recall that for the non-reactive case (Part 1), with $\beta = 0$ and $\phi = 1$, only a single subsonic neutral mode exists at $M = 0$, given by (3.1). We will show that the addition of heat release ($\beta > 0$) can cause multiple subsonic neutral modes to coexist, although the multiplicity may not always exist for all values of β. The original terminology from Part 1 was that 'fast' modes correspond to those found in region 2 of figure 2, and that 'slow' modes correspond to those found in region 4. We want to preserve this terminology in the current study. Since the flame sheet introduces several neutral modes in the subsonic region (region 1), we need to label these in such a way as to be consistent with the labelling for regions 2 and 4. To this end, 'fast' modes now correspond to phase speeds $c_N > \frac{1}{2}$ in the subsonic region and their continuation into region 2, and similarly for the 'slow' modes.

It can be shown from (3.1), and from (2.6*b*), (2.7*b*) and (2.10), that fast subsonic neutral modes only exist for

$$\beta \geqslant 1 - \beta_T \phi, \tag{3.2}$$

with corresponding neutral phase speed

$$c_N = \frac{\beta + \beta_T \phi}{\beta + (1 + \beta_T)\phi}, \tag{3.3}$$

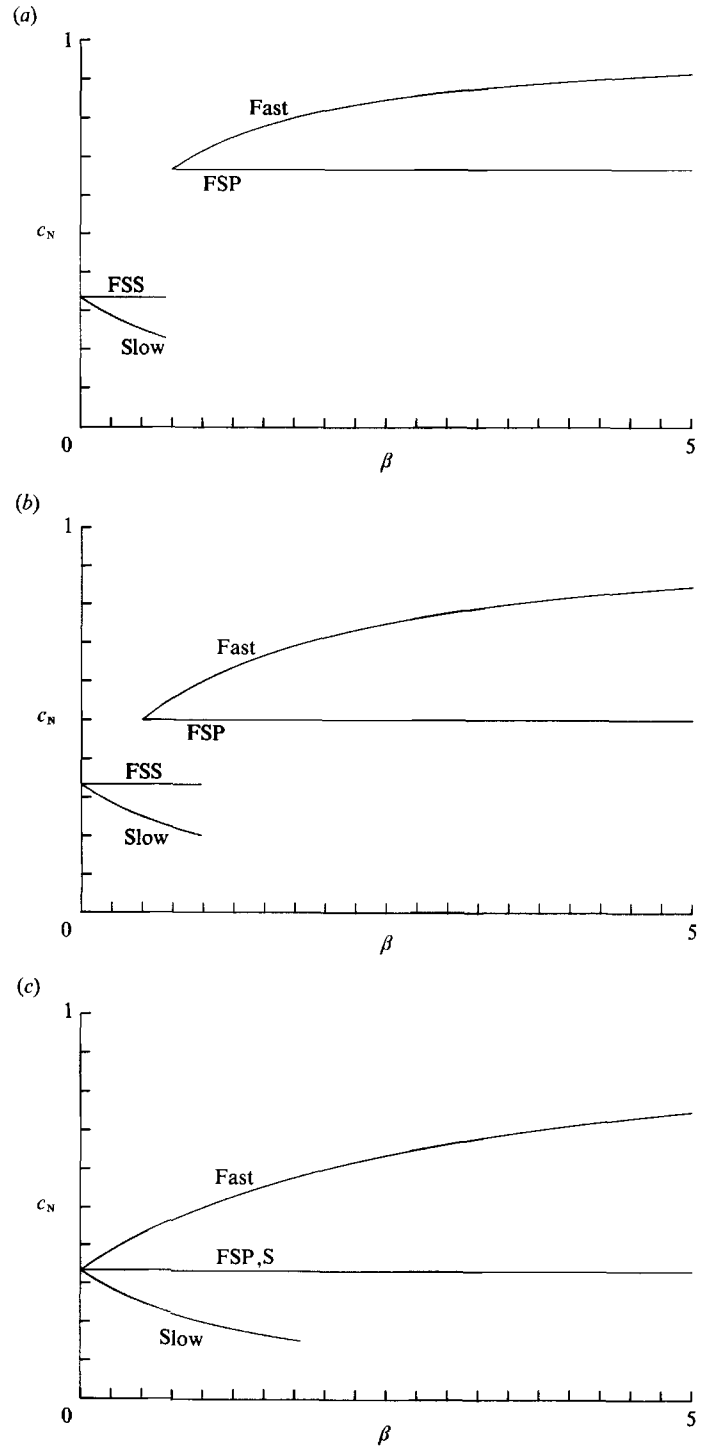

FIGURE 5. (*a*) Plot of neutral phase speeds c_N versus β for $\beta_T = 0.5$, $\phi = 0.5$, and $M = 0$. (*b*) Plot of neutral phase speeds c_N versus β for $\beta_T = 0.5$, $\phi = 1$, and $M = 0$. (*c*) Plot of neutral phase speeds c_N versus β for $\beta_T = 0.5$, $\phi = 2$, and $M = 0$.

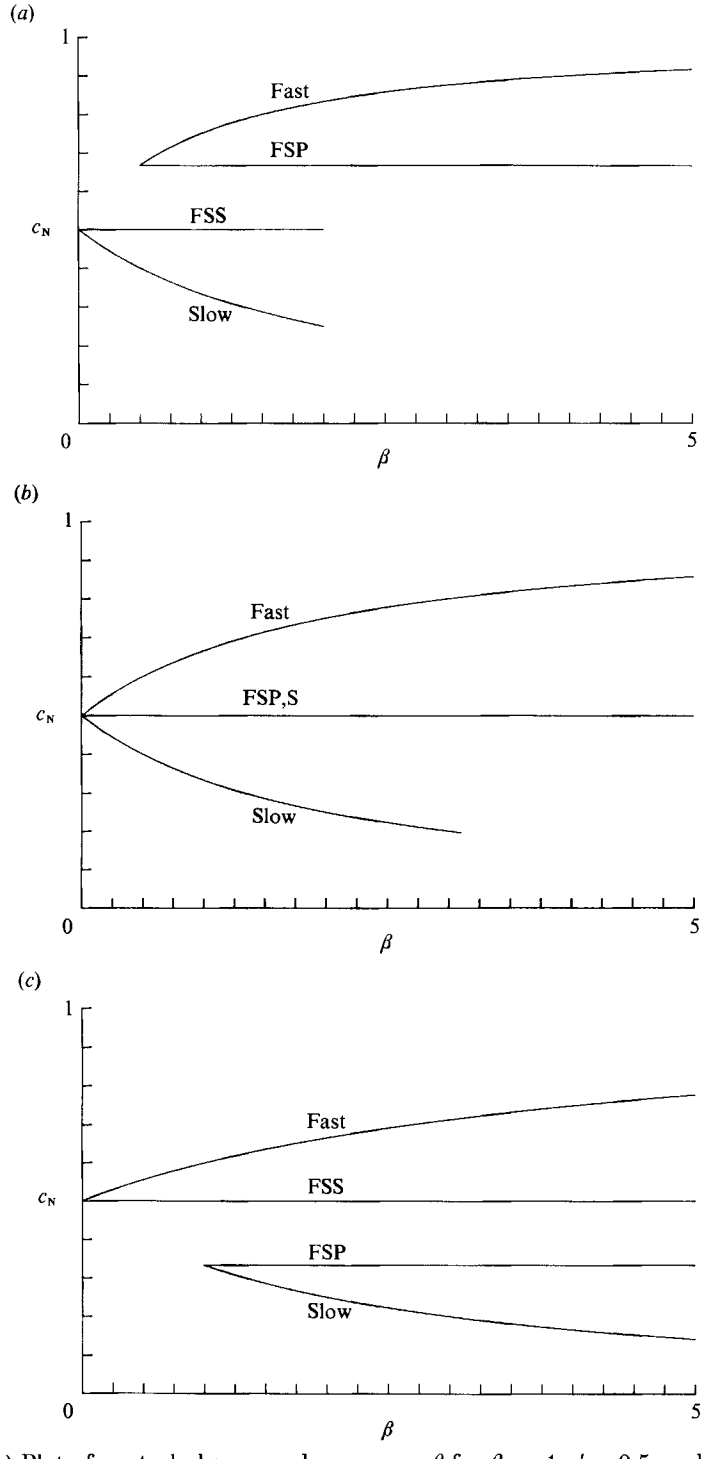

FIGURE 6. (*a*) Plot of neutral phase speeds c_N versus β for $\beta_T = 1$, $\phi = 0.5$, and $M = 0$. (*b*) Plot of neutral phase speeds c_N versus β for $\beta_T = 1$, $\phi = 1$, and $M = 0$. (*c*) Plot of neutral phase speeds c_N versus β for $\beta_T = 1$, $\phi = 2$, and $M = 0$.

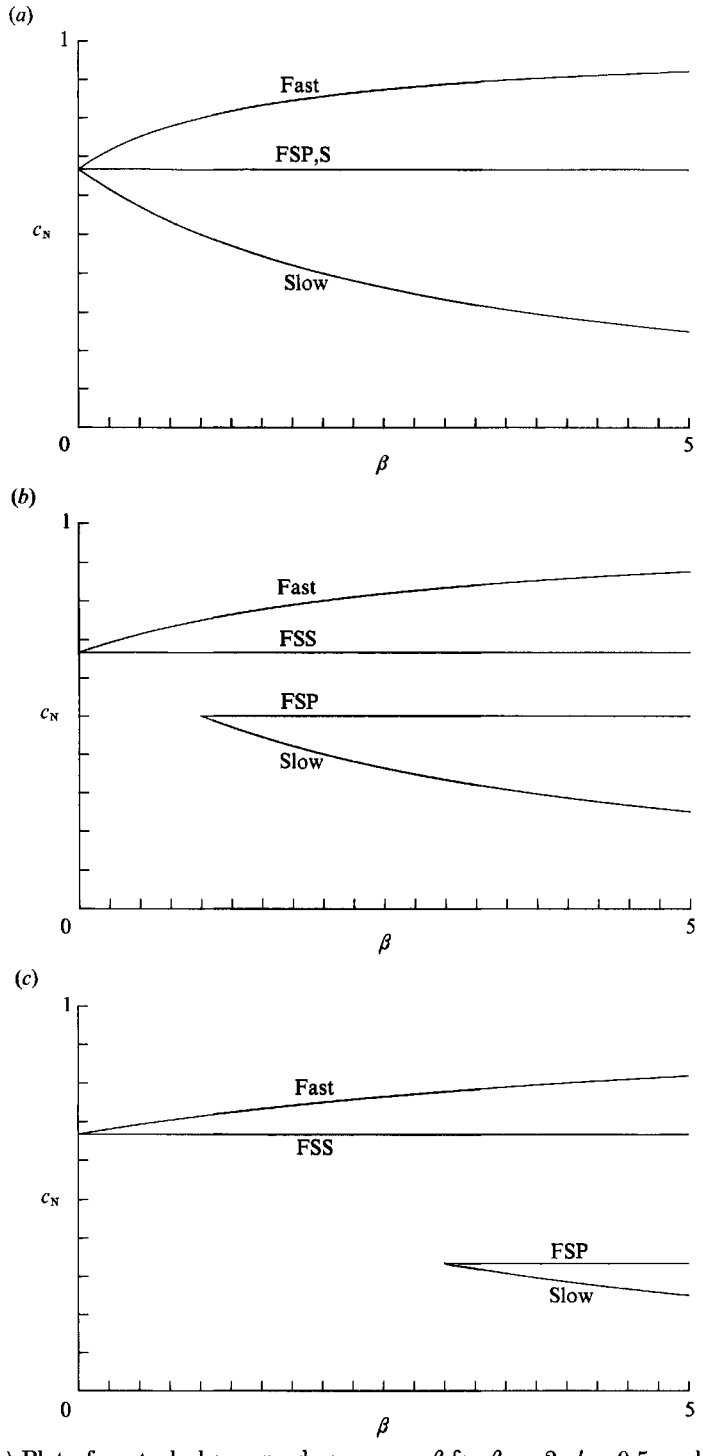

FIGURE 7. (*a*) Plot of neutral phase speeds c_N versus β for $\beta_T = 2$, $\phi = 0.5$, and $M = 0$. (*b*) Plot of neutral phase speeds c_N versus β for $\beta_T = 2$, $\phi = 1$, and $M = 0$. (*c*) Plot of neutral phase speeds c_N versus β for $\beta_T = 2$, $\phi = 2$, and $M = 0$.

while slow subsonic neutral modes only exist for

$$\beta \geqslant \beta_T \phi - 1, \tag{3.4}$$

with corresponding neutral phase speed

$$c_N = \frac{\beta_T}{1+\beta+\beta_T}. \tag{3.5}$$

Note that the value of the slow subsonic neutral phase speed is independent of the equivalence ratio ϕ. Also, note, from (3.2) and (3.4), that there is a mode switch located at $\beta = 0$ and $\phi = \beta_T^{-1}$; i.e. the modes interchange their characteristics at $\beta = 0$.

The phase speeds of the neutral modes for $\beta_T = 0.5$ are plotted in figure 5. Note that there are both fast and slow subsonic neutral modes whose phase speeds are given by (3.3) and (3.5). In addition to these subsonic neutral modes, there are adjacent neutral modes whose phase speeds are not given by (3.3) or by (3.5). These neutral modes are present because of the flame sheet, and for this reason we will call them 'flame sheet neutral modes'. They are characterized by having zero frequencies and zero wavenumbers. Their phase speeds are found numerically in the limit process $\alpha \to 0$. The phase speeds of one of these flame sheet modes was found to be $c_N = U(\eta_f)$, and so we classify it as the primary flame sheet neutral mode (denoted by FSP in the figures). The other flame sheet neutral mode always has the phase speed value which existed at $\beta = 0$, and we call this the secondary flame sheet neutral mode (denoted by FSS in the figures). For both the FSP and the FSS, their phase speeds are independent of β. As will be shown later, they are also independent of the Mach number. This is due to the fact that the flame location η_f is also independent of β_T and M. In either case, the eigenfunction structure is given by Π = constant. Curves of the phase speed of the neutral modes are only shown for those values of β for which the corresponding unstable modes are convectively unstable. It is clear from the results shown here and in figure 4 that it is the slow modes which becomes absolutely unstable when $\beta > \beta_c$ and that β_c increases with increasing values of the equivalence ratio ϕ. The fast modes, on the other hand, only exist for those values of β which satisfy (3.2). From figure 5(*c*) one can see that there will be a mode switch for $\phi > 2$ at $\beta = 0$. The phase speeds of the neutral modes for $\beta_T = 1$ are plotted in figure 6. Again we see that there are both fast and slow subsonic neutral modes with adjacent flame sheet neutral modes. Note that there is a mode switch at $\beta = 0$ as ϕ is increased past one. That is, for $\phi < 1$, only the slow modes exist at $\beta = 0$, and conversely for $\phi > 1$. As for the case of $\beta_T = 0.5$, only the slow modes undergo the transition from convective to absolute instability at $\beta = \beta_c$. Finally, figure 7 shows the variation of the phase speed with β for $\beta_T = 2$. The mode switch occurs when ϕ exceeds 0.5. It is clear that β_c is greater than 5 for all values of ϕ for which results are shown here and thus there is no transition from convective to absolute instability in this range of parameters.

3.1.2. *Unstable modes*

In addition to the neutral modes there are, of course, associated unstable modes. The maximum growth rates of the unstable modes for various values of β_T and ϕ are plotted as a function of β in figures 8–10. It is important to note the changes of scale between these figures.

In figure 8 the variation of $-\alpha_{i_{max}}$ with β is shown for $\beta_T = 0.5$ and $\phi = 0.5, 1, 2$. The slow modes are much more unstable than the fast modes for those ranges of β

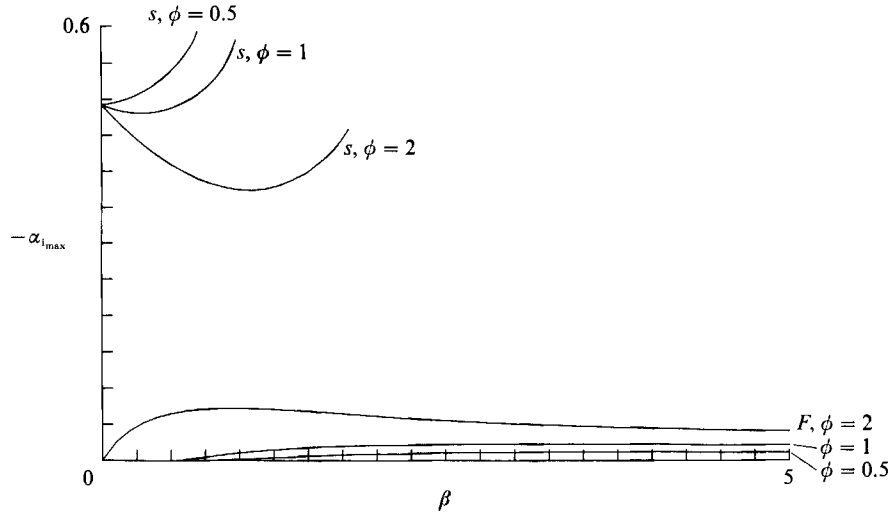

FIGURE 8. Plot of maximum growth rates of the fast and slow modes versus β for $\beta_T = 0.5$, $\phi = 0.5, 1, 2$, and $M = 0$.

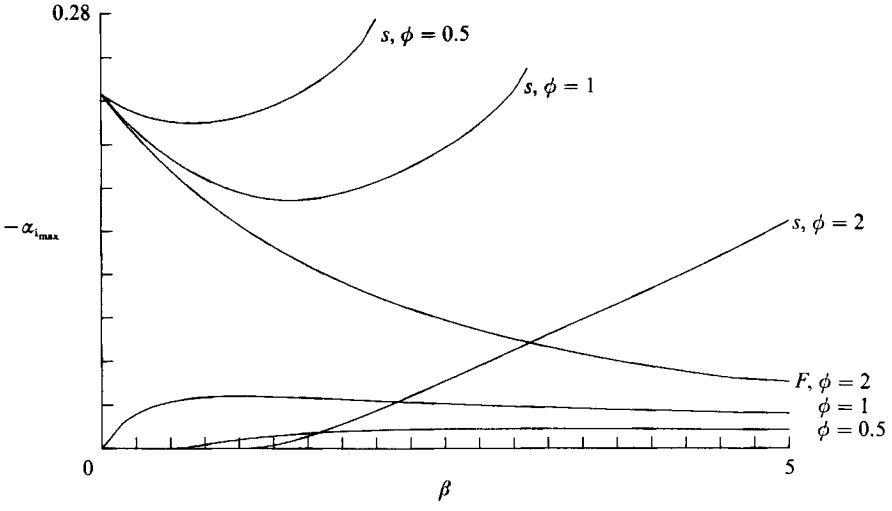

FIGURE 9. Plot of maximum growth rates of the fast and slow modes versus β for $\beta_T = 1$, $\phi = 0.5, 1, 2$, and $M = 0$.

for which the slow modes are convectively unstable, i.e. $\beta < \beta_c$. The maximum growth rates of these slow modes first decrease slightly and then increase with an increase in β. The maximum growth rates of the fast modes increase with ϕ for any β but are much smaller than those of the slow modes. Similar results are shown in figure 9 for $\beta_T = 1$. The switching between fast and slow modes past $\phi = 1$ which was noted in our discussion of the phase speeds of the neutral modes is apparent in this figure. The growth rates of the fast waves increase with ϕ, while those of the slow waves decrease. Finally the plots of the maximum growth rate versus β for $\beta_T = 2$, shown in figure 10, have the same general behaviour as the two previous figures. That is, there is a mode switch at $\beta = 0$ past $\phi = \frac{1}{2}$.

The results shown in these figures can be summarized as follows. An increase in β_T causes a decrease in the maximum growth rate of the most unstable modes. At fixed

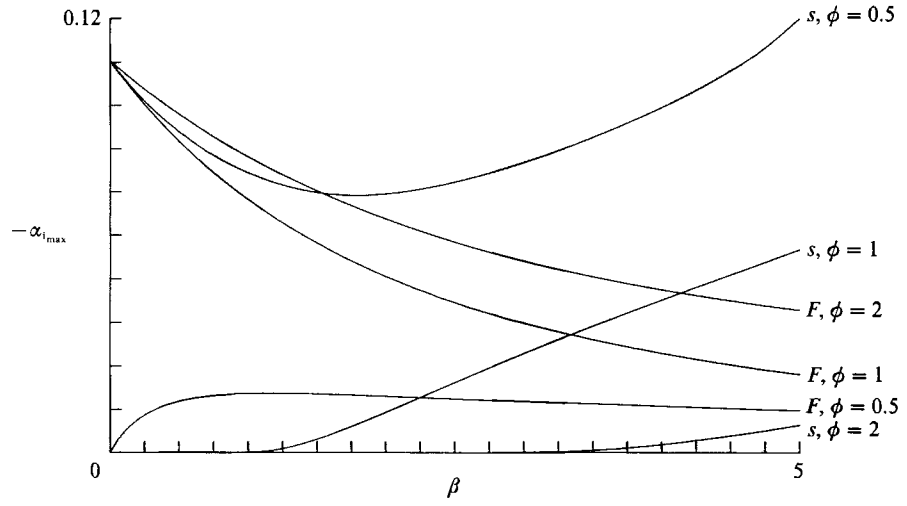

FIGURE 10. Plot of maximum growth rates of the fast and slow modes versus β for $\beta_T = 2$, $\phi = 0.5, 1, 2$, and $M = 0$.

β_T and ϕ the growth rate of the slow modes increases as β becomes large as long as the flow is convectively unstable, while the growth rate of the fast modes approaches a limiting value. As we shall see, this is the same generic behaviour as results from increasing the Mach number while holding all other parameters fixed. Thus, for sufficiently large β, the slow modes are the most unstable ones, unless there is a transition from convective to absolute instability. For fixed β, an increase in ϕ causes an increase in the maximum growth rates of the fast modes, while decreasing the maximum growth rates of the slow modes. Finally, we have found that the phase speeds c_{ph} of the unstable modes lie between the phase speed of the subsonic neutral mode and its adjacent flame sheet neutral mode.

3.2. $M > 0$

In this section we show the variation of the phase speeds of the neutral waves and the maximum growth rates of the unstable waves as a function of the Mach number for various combinations of β_T, β, and ϕ.

3.2.1. *Neutral modes*

In figure 11 (*a*) we show the phase speed of the neutral modes for the non-reactive ($\beta = 0, \phi = 1$) mixing layer (Part 1) for $\beta_T = \frac{1}{2}$. From this figure, taken from Part 1, one can see that there is only a single subsonic neutral mode in region 1. This mode crosses over the sonic curve at M_s, the Mach number at which the phase speed equals that of a sonic wave, and is transformed into a supersonic neutral mode in region 4. In addition, a fast supersonic neutral mode appears at M_* in region 2. In regions 2 and 4 there are unstable modes with phase speeds between that of the supersonic neutral mode and that of the sonic neutral mode. Thus, there are two bands of unstable frequencies for Mach numbers greater than M_*. The band in region 2 is a group of fast and the band in region 4 is a group of slow unstable modes. The phase speeds of both the fast and slow modes have a small range about the average, so that little dispersion of wave packets is expected, with a reduction in the dispersion as the Mach number is increased.

It can be seen from figure 11 (*b*) that chemical reaction has a major effect on c_N.

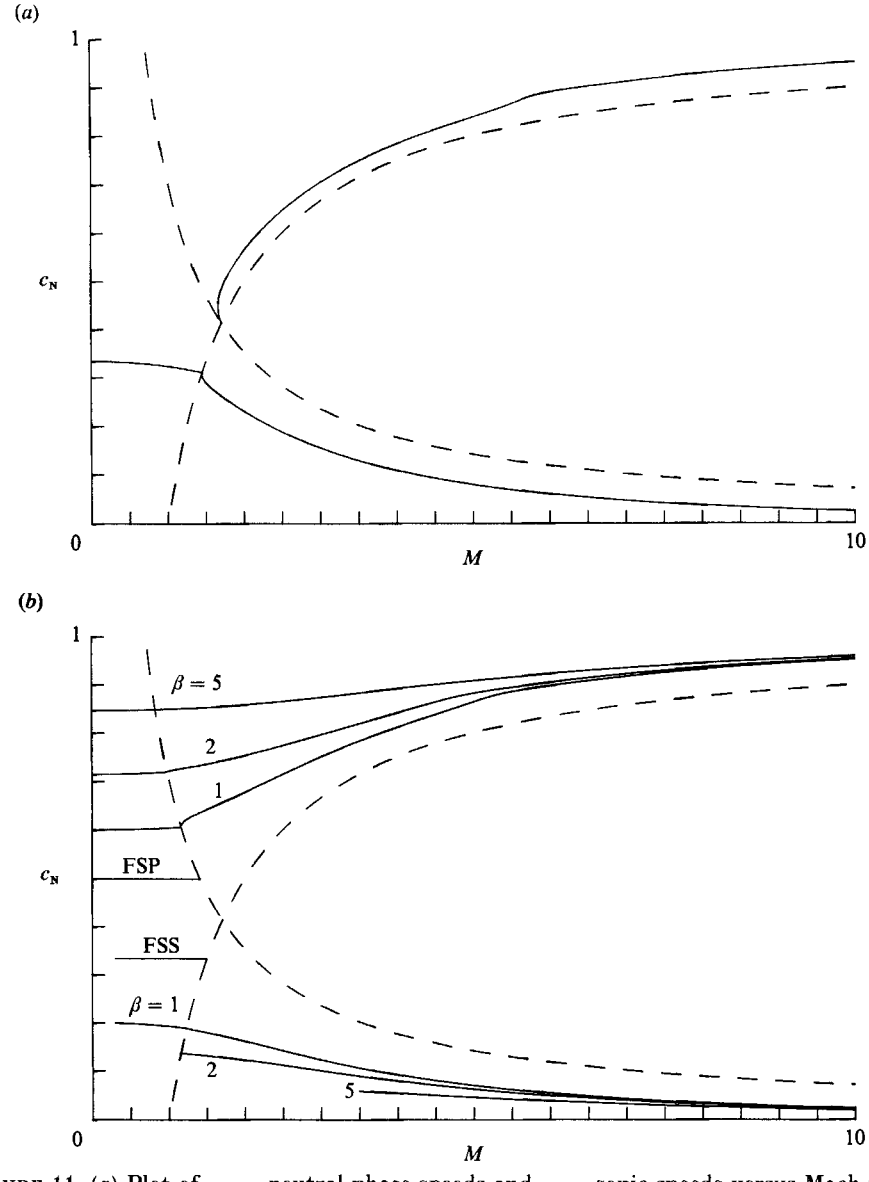

FIGURE 11. (*a*) Plot of ——, neutral phase speeds and – – –, sonic speeds versus Mach number for $\beta_T = 0.5$, $\beta = 0$, and $\phi = 1$. (*b*) Plot of ——, neutral phase speeds and – – –, sonic speeds versus Mach number for $\beta_T = 0.5$, $\beta = 1, 2, 5$, and $\phi = 1$.

First, recall from figure 5(*b*) that the slow subsonic neutral mode is convectively unstable only for $\beta < \beta_c$ at $M = 0$, while the fast subsonic neutral mode only exists for $\beta \geqslant \frac{1}{2}$. As can be seen from figure 4(*c*), the value of β_c is also a function of the Mach number. Thus, we find that the slow neutral mode is convectively unstable only if the Mach number is greater than the critical value M_c (see figure 11*b*). Apart from this, the values of c_N on this branch are only slightly affected by changes in β and the effect is quite small at large M. Finally, one can see that a fast subsonic neutral mode is present for all M because β is greater than 0.5. Note that the values of c_N for this fast mode in region 1 increase markedly with increasing β. This is also true for the lower

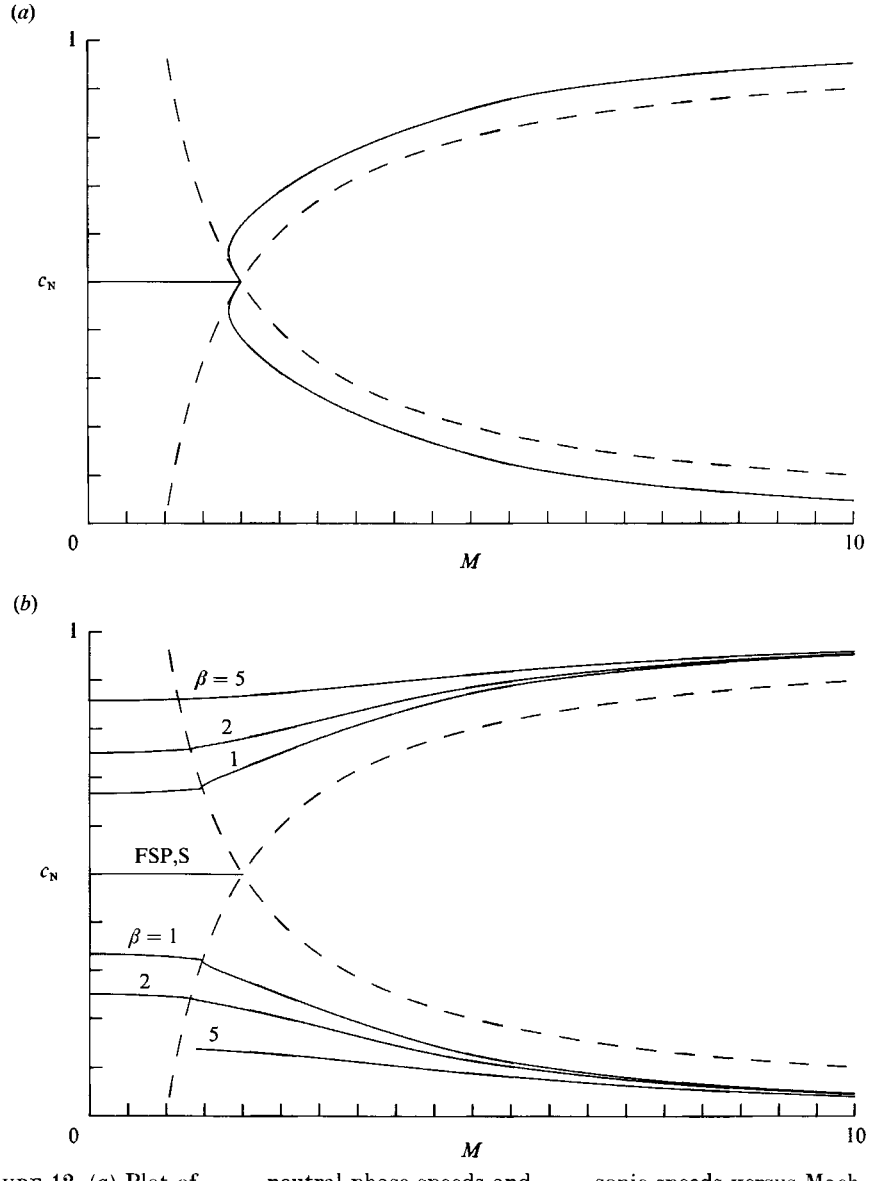

FIGURE 12. (*a*) Plot of ——, neutral phase speeds and – – –, sonic speeds versus Mach number for $\beta_T = 1$, $\beta = 0$, and $\phi = 1$. (*b*) Plot of ——, neutral phase speeds and – – –, sonic speeds versus Mach number for $\beta_T = 1$. $\beta = 1, 2, 5$, and $\phi = 1$.

Mach number range in region 2, but all of the c_N curves for different β appear to asymptote to a single curve for large M. Associated with the fast and slow subsonic neutral modes there are the flame sheet neutral modes in region 1. The range of phase speeds of the unstable modes in region 1 lies between the fast modes and their associated flame sheet mode, and between the slow modes and their associated flame sheet mode. In regions 2 and 4, the range of phase speeds of the unstable modes lies between the fast (slow) supersonic neutral modes and the associated fast (slow) sonic neutral modes. The range of the phase speeds of the unstable modes increases with β and is quite large for Mach numbers around M_*, thus yielding an increase in

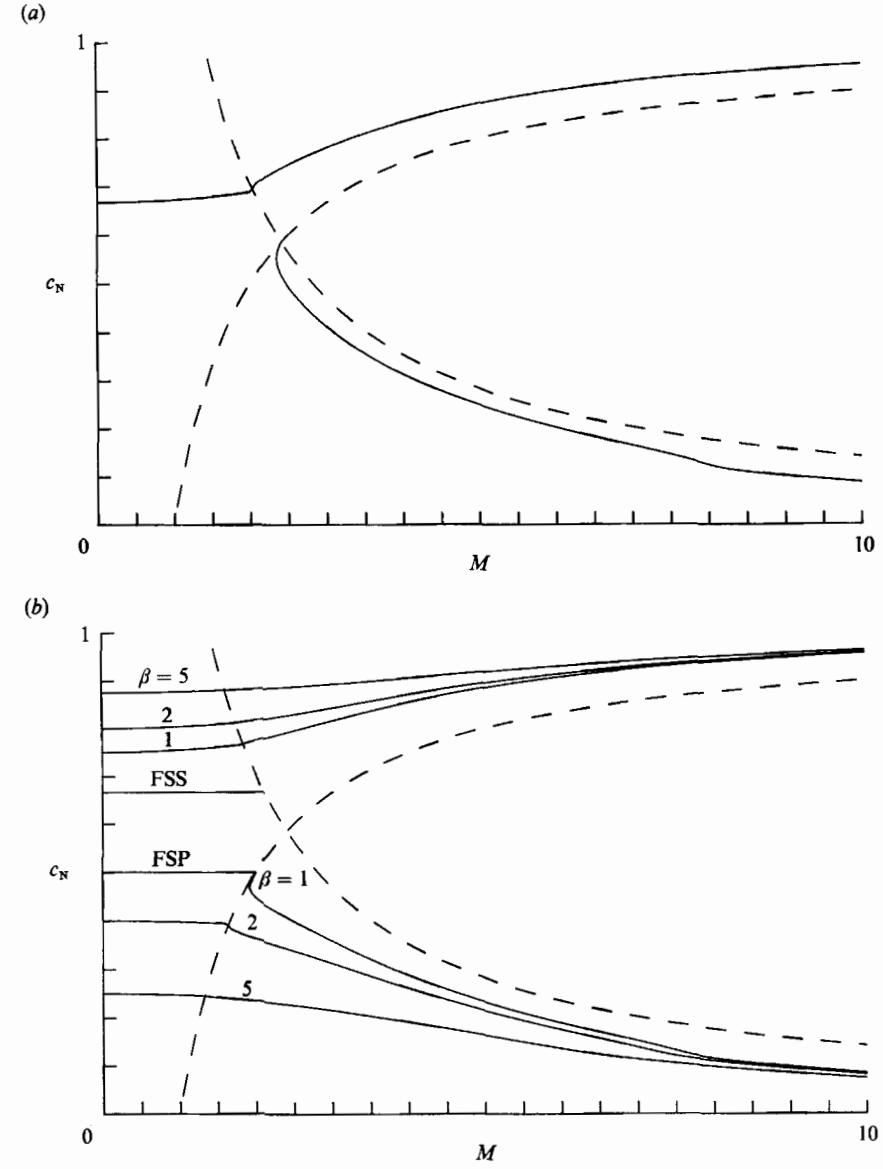

FIGURE 13. (*a*) Plot of ——, neutral phase speeds and – – –, sonic speeds versus Mach number for $\beta_T = 2$, $\beta = 0$, and $\phi = 1$. (*b*) Plot of ——, neutral phase speeds and – – –, sonic speeds versus Mach number for $\beta_T = 2$, $\beta = 1, 2, 5$, and $\phi = 1$.

dispersion. However for Mach numbers much larger than M_* the dispersion is essentially independent of β.

Figure 12 shows the phase speed of the neutral modes for $\beta_T = 1, \phi = 1$ and various values of β as a function of the Mach number. The results for $\beta = 0$ are shown in figure 12(*a*) and those for $\beta > 0$ in figure 12(*b*). The curves of c_N versus M are symmetric about the line $c_N = \frac{1}{2}$ because the mean velocity profile is symmetric about $\eta = 0$ (where $U = \frac{1}{2}$) and so is the temperature profile for any β if $\phi = 1$. Hence, the subsonic neutral mode in region 1 of figure 12(*a*) splits into a symmetric pair of fast and slow supersonic modes at M_*. From figure 12(*b*) it can be seen that this is also

true for any non-zero β. The only exception is for sufficiently large β, where the slow neutral modes are convectively unstable only if the Mach number exceeds M_c. For this case, the flame sheet neutral mode in region 1 has a phase speed of $\frac{1}{2}$, and the range of phase speeds of the unstable modes lies between this mode and the corresponding fast and slow neutral modes. As β increases the phase speeds of the fast (slow) neutral modes increase (decrease) at any fixed M. Again it should be noted that all of the curves for both the fast and slow neutral modes at different β are asymptotic to a single curve for large M. As for the previous case, an increase in β causes an increase in the range of the phase speeds of the unstable modes, in the vicinity of M_*, and hence an increase in the dispersion.

Finally, in figure 13 we show similar plots of c_N versus M for $\beta_T = 2$. In figure 13(*a*), with $\beta = 0$, there is only a subsonic fast neutral mode in region 1 which is transformed into a supersonic neutral mode in region 2. The slow supersonic neutral mode only exists in region 4. The effects of increasing β are similar to those of the cases discussed above. There is an increase in the phase speed of the fast modes as β is increased. The phase speed of the slow supersonic modes of region 4 decreases with increasing β and, for $\beta > 1$, a flame sheet neutral mode with $c_N = \frac{1}{2}$ appears in region 1. Correspondingly, for $\beta > 0$, there also exists a flame sheet neutral mode in region 1 associated with the fast modes. Again the curves for the fast and slow neutral modes are each asymptotic to a single curve for large M. As in the previous two cases, an increase in β causes an increase in the range of the phase speeds of the unstable waves and hence an increase in the dispersion.

We have also carried out calculations of c_N versus M for fixed β_T and β with various values of ϕ. The results can be easily summarized. As ϕ increases the phase speed of the slow mode is unchanged, consistent with the Mach zero results (see equation (3.5)). The only effect is a change in the critical value of M_c below which the mode is absolutely unstable; the smaller the value of ϕ the smaller is the value of M_c. The phase speed of the fast neutral modes decreases with increasing ϕ. Finally, all of these curves appear to be asymptotic to a single curve as $M \to \infty$.

3.2.2. *Unstable modes*

In addition to the phase speeds we have calculated the maximum growth rates of the unstable modes for these values of β_T, β, and ϕ as a function of the Mach number. The results are shown in figures 14–16. Again, it is important to note the changes of scales between these figures.

The maximum growth rate as a function of M with $\beta_T = \frac{1}{2}$, $\phi = 1$ and various β is plotted in figure 14(*a*). For $\beta = 0$ an increase in the Mach number from zero results in a decrease in the growth rate of the slow mode by a factor of five to ten up to M_*, and for higher Mach numbers the growth rate levels off and eventually begins to increase with increasing Mach number. An increase in β causes the growth rate of the slow modes to increase, but the variation of the growth rate with M is similar to that for $\beta = 0$. However, it must be recalled that, if $\beta > 0$, the slow modes are convectively unstable only for Mach numbers greater than M_c, and this is reflected in the curves for $\beta > 0.984$. The growth rates of the fast modes are much smaller and increasing β has only a slight effect on them. Figure 14(*b*) contains similar results, but with $\beta = 2$ and varying ϕ. An increase in ϕ causes an increase in the maximum growth rate of the slow modes and a decrease for the fast modes at low and moderate Mach numbers. At higher Mach numbers, the growth rates are essentially independent of ϕ.

Similar results, but with $\beta_T = 1$, are given in figure 15. It can be seen that the

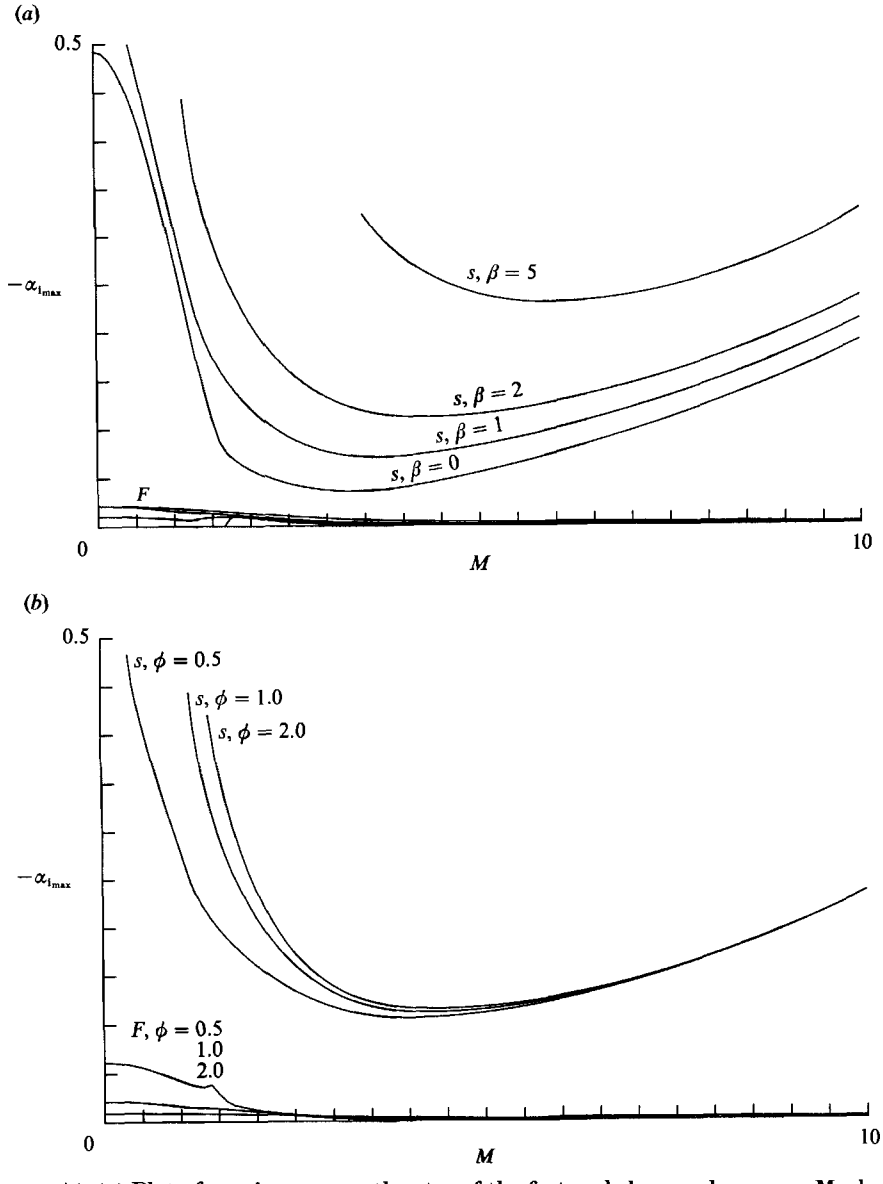

FIGURE 14. (*a*) Plot of maximum growth rates of the fast and slow modes versus Mach number for $\beta_T = 0.5$, $\beta = 0, 1, 2, 5$, and $\phi = 1$. (*b*) Plot of maximum growth rates of the fast and slow modes versus Mach number for $\beta_T = 0.5$, $\beta = 2$, and $\phi = 0.5, 1, 2$.

effects of varying β on the growth rate (figure 15*a*) is somewhat more complex than for the previous case. The maximum growth rate of the slow modes at low Mach numbers first decreases and then increases with increasing β, consistent with the Mach zero results of figure 9. At higher Mach numbers, increasing β causes a monotonic increase in the maximum growth rates of the slow modes. Again there is a five- to ten-fold decrease in the growth rates of the slow modes as the Mach number increases from zero to M_*, and a slight increase at higher Mach numbers. Apart from the appearance of the fast modes at low Mach number, increasing β has little effect on their maximum growth rates. Finally, in figure 15(*b*), an increase in ϕ with fixed

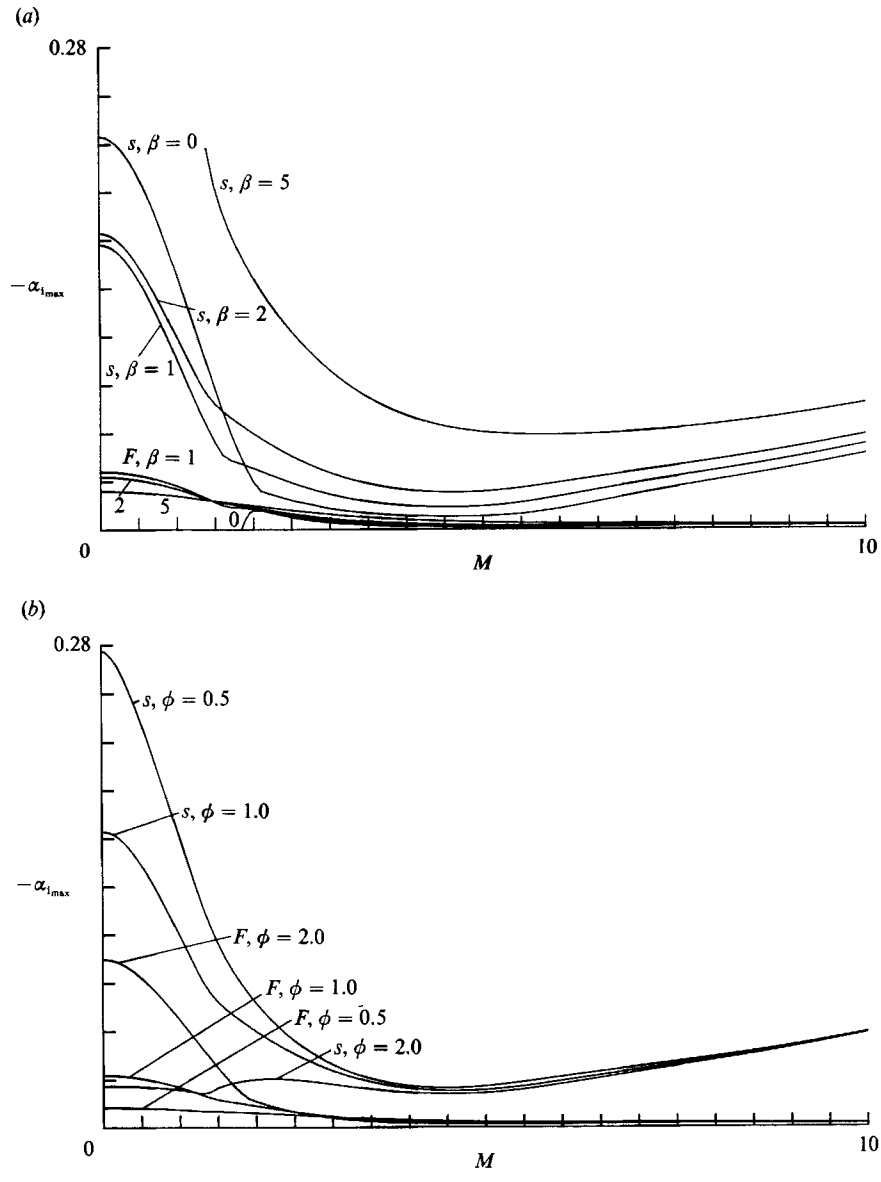

FIGURE 15. (*a*) Plot of maximum growth rates of the fast and slow modes versus Mach number for $\beta_T = 1$, $\beta = 0, 1, 2, 5$, and $\phi = 1$. (*b*) Plot of maximum growth rates of the fast and slow modes versus Mach number for $\beta_T = 1$, $\beta = 2$, and $\phi = 0.5, 1, 2$.

β results in an increase in the maximum growth rate of the fast modes and a decrease in the maximum growth rate of the slow modes at low and moderate Mach numbers. At higher Mach numbers, the growth rates are again independent of ϕ.

In figure 16 similar results are given for $\beta_T = 2$. These results are consistent with the Mach zero results of figure 10. In particular, figure 16(*a*) shows that the slow modes are strictly increasing and those of the fast modes are strictly decreasing with increasing β at zero Mach number. Thus, increasing β causes a substantial decrease in the maximum growth rates of the fast modes and a substantial increase in the maximum growth rates of the slow modes at low and moderate Mach numbers. As

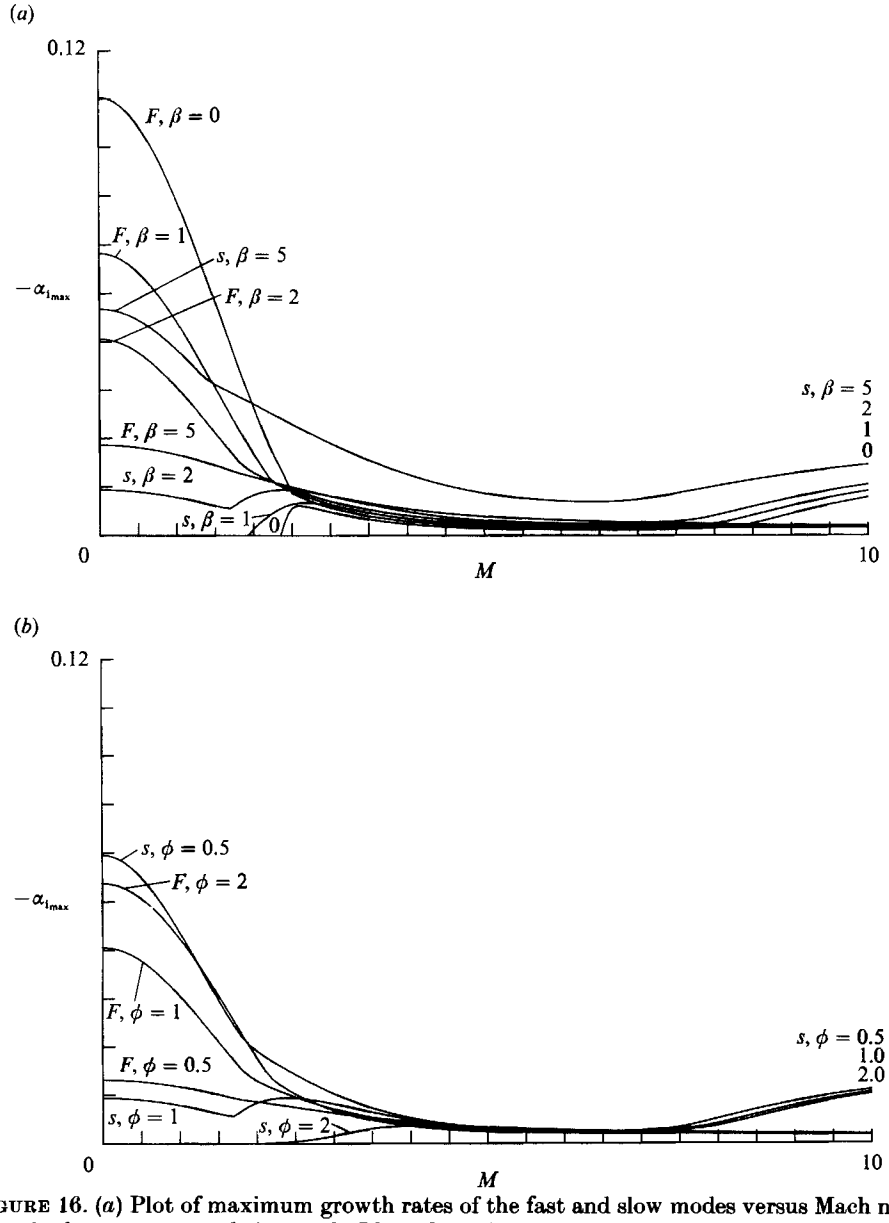

FIGURE 16. (*a*) Plot of maximum growth rates of the fast and slow modes versus Mach number for $\beta_T = 2$, $\beta = 0, 1, 2, 5$, and $\phi = 1$. (*b*) Plot of maximum growth rates of the fast and slow modes versus Mach number for $\beta_T = 2$, $\beta = 2$, and $\phi = 0.5, 1, 2$.

in the previous case, the results of figure 16(*b*) show that increasing ϕ yields an increase in the growth rates of the fast modes while decreasing those of the slow modes. As before, the growth rates of both are independent of ϕ at higher Mach number.

The results presented in figures 14–16 thus show that the maximum growth rates of the slow modes increase as the Mach number becomes large, while that of the fast modes approaches a limiting value. As we have seen, this was the same generic behaviour as results from increasing the heat release parameter β at zero Mach number.

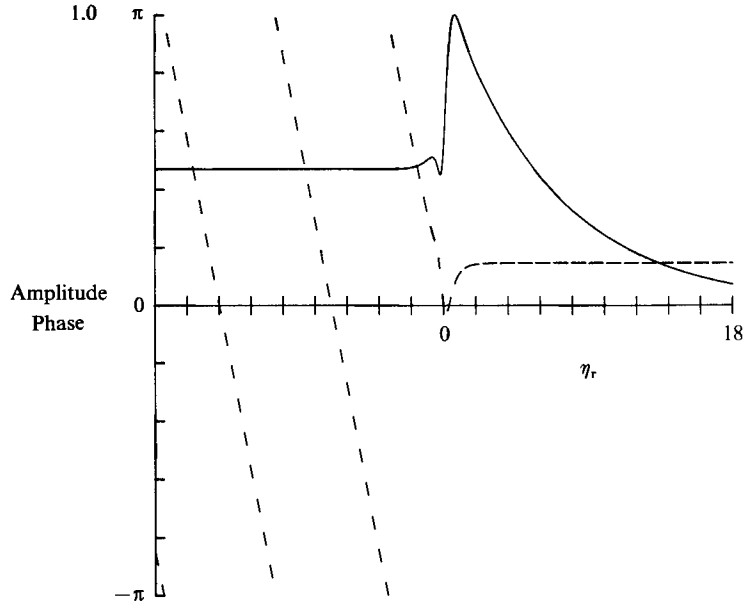

FIGURE 17. Plot of the two dimensional fast supersonic neutral eigenfunction $\Pi(\eta)$ along the contour $\eta = \eta_r - i$. The solid curve corresponds to the amplitude and the dashed curve to the phase. $M = 5$, $\beta_T = 1$, $\phi = 1$, $\beta = 0$, with $\omega_N = 0.184813$, $\alpha_N = 0.215661$, $c_N = 0.85696$.

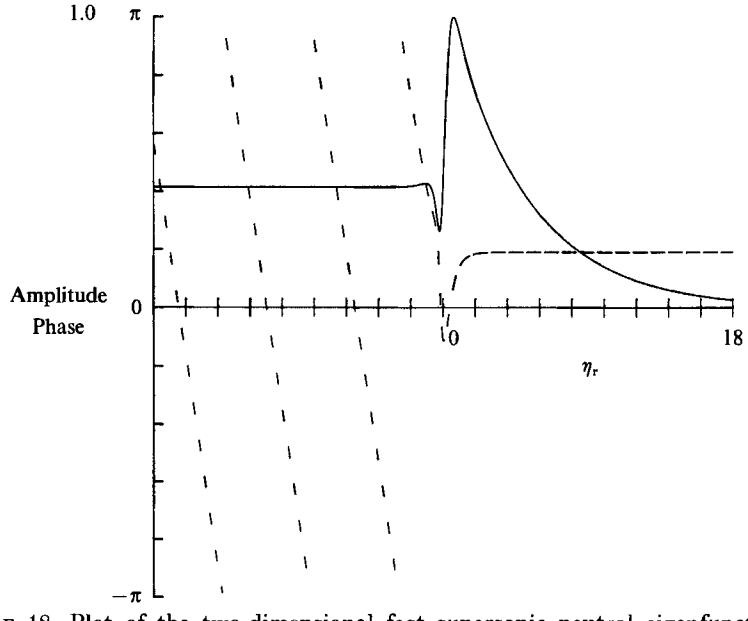

FIGURE 18. Plot of the two-dimensional fast supersonic neutral eigenfunction $\Pi(\eta)$ along the contour $\eta = \eta_r - i$. The solid curve corresponds to the amplitude and the dashed curve to the phase. $M = 5$, $\beta_T = 1$, $\phi = 1$, $\beta = 1$, with $\omega_N = 0.235413$, $\alpha_N = 0.269485$, $c_N = 0.873565$.

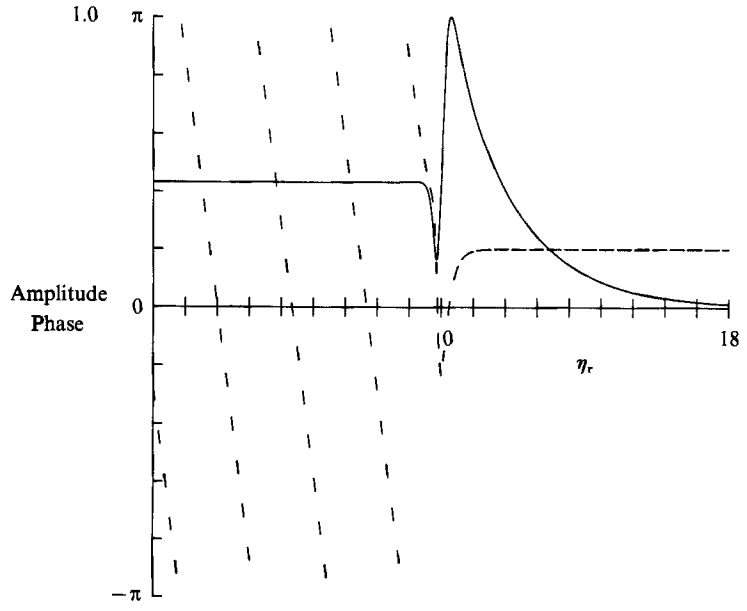

FIGURE 19. Plot of the two-dimensional fast supersonic neutral eigenfunction $\Pi(\eta)$ along the contour $\eta = \eta_r - i$. The solid curve corresponds to the amplitude and the dashed curve to the phase. $M = 5$, $\beta_T = 1$, $\phi = 1$, $\beta = 2$, with $\omega_N = 0.276698$, $\alpha_N = 0.312299$, $c_N = 0.886001$.

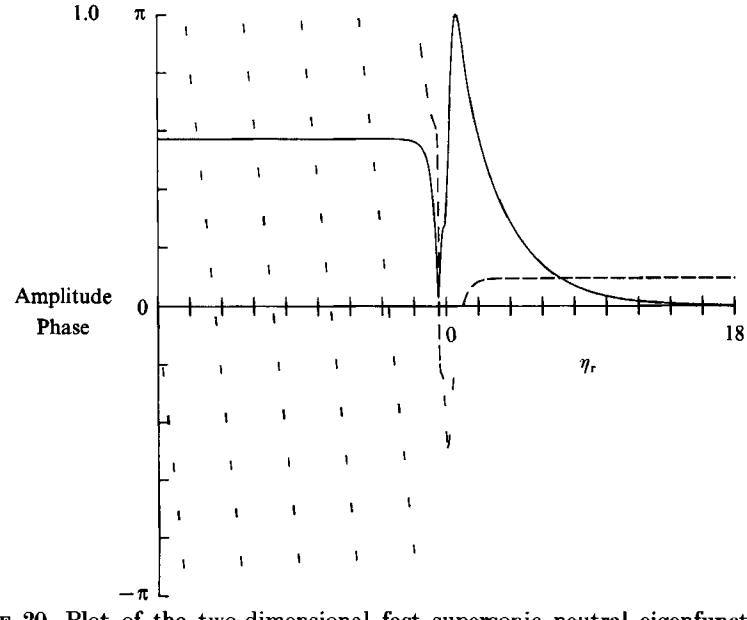

FIGURE 20. Plot of the two-dimensional fast supersonic neutral eigenfunction $\Pi(\eta)$ along the contour $\eta = \eta_r - i$. The solid curve corresponds to the amplitude and the dashed curve to the phase. $M = 5$, $\beta_T = 1$, $\phi = 1$, $\beta = 5$, with $\omega_N = 0.356124$, $\alpha_N = 0.390535$, $c_N = 0.911887$.

3.2.3. *Neutral eigenfunctions*

Figures 17–20 are plots of selected two-dimensional neutral eigenfunctions for $\beta_T = 1, \phi = 1$, Mach 5 and increasing values of β. These plots show the variation of Π with η_r on the contour $\eta_i = -1$. All of these have been normalized so that the maximum of the absolute value of Π is unity. The eigenfunctions shown are all fast supersonic neutral modes whose phase speeds are shown in figure 12. Note the rapid variation of both the amplitude and phase near $\eta_r = 0$. Because these modes are fast, they show exponential decay in the subsonic region and oscillations with constant amplitude and linear phase in the supersonic region. As β is increased, the variation of the amplitude near $\eta_r = 0$ increases markedly. Also, the decay of the amplitude in the subsonic region is more rapid and the rate of change of the phase in the supersonic region increases. The behaviour of the eigenfunction with increasing heat release, β, is similar to the behaviour with increasing Mach number.

4. Conclusions

The addition of combustion in the form of a flame sheet has important, and complex, effects on the flow stability. We have found that the addition of heat can cause the compressible mixing layer to become absolutely unstable even without any reversed flow. This transition occurs at a critical value of β (β_c) which depends upon the Mach number, β_T, and ϕ. Thus it is possible to induce absolute instability by either increasing the heat release parameter β, or by decreasing the equivalence ratio ϕ (i.e. lean mixtures), holding all other parameters fixed. However, increasing the Mach number and/or increasing β_T causes β_c to increase, and thus it is possible to regain a convectively unstable flow. We have only reported results for modes which are convectively unstable. In this flow there can be multiple groups of unstable waves. In some cases, one of these is absolutely unstable and the others are convectively unstable. It may not be possible to observe these convectively unstable modes because of the presence of the absolute instability. Nevertheless we have reported phase speeds and growth rates for them.

In contrast to the non-reacting case, we have shown the existence of multiple subsonic neutral modes in region 1. For Mach numbers greater than M_*, there are two bands of unstable frequencies (just as in the non-reacting case); one a group of fast supersonic modes and the other a group of slow supersonic modes. In general, an increase in β causes an increase (decrease) in the phase speed of the fast (slow) neutral modes. Since the range of phase speeds is increased at low and moderate Mach numbers as the heat release parameter β is increased, there is an increase in the dispersion of wave packets. Finally, we have found that the addition of chemical heating has almost no effect on the neutral phase speeds at higher Mach numbers.

The maximum growth rates of the unstable modes decrease by a factor of five to ten as the Mach number approaches M_*, even with the presence of the reaction. Just as in the non-reacting case, for Mach numbers greater than M_*, the growth rates level off and those of the slow modes eventually begin to increase with increasing Mach number, while the growth rates of the fast modes approach a limiting value. The same behaviour results from increasing β while the Mach number is held fixed. Finally, if the stationary gas is colder than the moving gas, $\beta_T < 1$, the effect of increasing the equivalence ratio ϕ is to increase the growth rate of the slow modes and decrease the growth rate of the fast modes. On the other hand, if $\beta_T \geqslant 1$, increasing ϕ has the opposite effect. However, at higher Mach numbers, changes in

ϕ have little effect on the growth rates for any β_T. Finally, an examination of the eigenfunctions shows that increasing β has the same generic effect as increasing the Mach number.

The general trends that we have found of the effect of heat release on the overall growth rate of the mixing layer are in agreement with the results of the studies of Hermanson & Dimotakis (1989) and McMurtry *et al.* (1989). We note that McMurtry *et al.* (1989) suggest that high rates of heat release may enhance mixing in the shear layer. We conjecture that this may be related to a transition from convective to absolute instability.

This study is the only comprehensive study, of which we know, of the inviscid spatial stability of a reacting compressible mixing layer. We do not know how sensitive our results are to the assumptions used in this study. In particular, we have assumed unit Prandtl and Lewis numbers, used Chapman's linear relation between viscosity and temperature, and approximated the mean velocity profile by a hyperbolic tangent. In addition, we have taken the limit of infinite Damkohler number which reduces the diffusion flame to a flame sheet. Despite these limitations, we believe that this systematic study is an important first step in classifying and understanding the complex effects that chemistry has on the stability of compressible free shear layers. As mentioned above, the next step is to consider a more realistic model of the chemistry and the thermodynamics. This will then yield mean velocity, temperature, and mass fraction distributions which will be continuous and have continuous derivatives across the flame. However the calculation of the mean field as well as the perturbation solution will be more difficult since now the velocity, temperature, and mass fraction equations are coupled. We have begun this study with finite Damkohler number and hope to report the results at a later date and will compare those results to the benchmark results reported here. The important question of absolute/convective instability also needs to be re-examined.

We wish to acknowledge helpful conversations and comments from J. P. Drummond. We also wish to acknowledge helpful comments from the referees, whose remarks have improved the paper. This work was supported by the National Aeronautics and Space Administration under NASA Contract Nos. NAS1-18107 and NAS1-18605 while the authors were in residence at the Institute for Computer Applications in Science and Engineering, NASA Langley Research Center, Hampton, VA 23665, USA.

REFERENCES

Brown, G. L. & Roshko, A. 1974 On density effects and large structure in turbulent mixing layers. *J. Fluid Mech.* **64**, 775–816.

Buckmaster, J. D. & Ludford, G. S. S. 1982 *Theory of Laminar Flames.* Cambridge University Press.

Chinzei, N., Masuya, G., Komuro, T., Murakami, A. & Kudou, D. 1986 Spreading of two-stream supersonic turbulent mixing layers. *Phys. Fluids* **29**, 1345–1347.

Drummond, J. P. & Mukunda, H. S. 1988 A numerical study of mixing enhancement in supersonic reacting flow fields. *AIAA paper* 88-3260.

Hermanson, J. C. & Dimotakis, P. E. 1989 Effects of heat release in a turbulent, reacting shear layer. *J. Fluid Mech.* **199**, 333–375.

Huerre, P. & Monkewitz, P. A. 1985 Absolute and convective instabilities in free shear layers. *J. Fluid Mech.* **159**, 151–168.

Jackson, T. L. & Grosch, C. E. 1989 Inviscid spatial stability of a compressible mixing layer. *J. Fluid Mech.* **208**, 609–637.

JACKSON, T. L. & GROSCH, C. E. 1990 Absolute/convective instabilities and the convective Mach number in a compressible mixing layer. *Phys. Fluids* A in press.

JACKSON, T. L. & HUSSAINI, M. Y. 1988 An asymptotic analysis of supersonic reacting mixing layers. *Comb. Sci. Tech.* **57**, 129–140.

KUMAR, A., BUSHNELL, D. M. & HUSSAINI, M. Y. 1987 A mixing augmentation technique for hypervelocity scramjets. *AIAA paper* 87-1882.

LEES, L. & LIN, C. C. 1946 Investigation of the stability of the laminar boundary layer in a compressible fluid. *NACA Tech. Note* 1115.

MACARAEG, M. G. & STREETT, C. L. 1990 Linear stability of high-speed mixing layers. To appear in a special issue of *Appl. Numer. Maths* (ed. M. Salas).

MACK, L. M. 1989 On the inviscid acoustic-mode instability of supersonic shear flows. *Fourth Symposium on Numerical and Physical Aspects of Aerodynamic Flows*, pp. 1–15. California State University, Long Beach, CA.

MCMURTRY, P. A., RILEY, J. J. & METCALFE, R. W. 1989 Effects of heat release on the large-scale structure in turbulent mixing layers. *J. Fluid Mech.* **199**, 297–332.

MENON, S., ANDERSON, J. D. & PAI, S. I. 1984 Stability of a laminar premixed supersonic free shear layer with chemical reactions. *Intl J. Engng Sci.* **22**(4), 361–374.

PAPAMOSCHOU, D. & ROSHKO, A. 1986 Observations of supersonic free-shear layers. *AIAA paper* 86-0162.

PAPAMOSCHOU, D. & ROSHKO, A. 1988 The compressible turbulent shear layer: an experimental study. *J. Fluid Mech.* **197**, 453–477.

PAVITHRAN, S. & REDEKOPP, L. G. 1990 The absolute-convective transition in subsonic mixing layers. *Phys. Fluids* A **1**, 1736–1739.

WILLIAMS, F. A. 1985 *Combustion Theory*, 2nd edn. Menlo Park, CA: Benjamin/Cummings.